TROLL 4.0: representing water and carbon fluxes, leaf phenology, and intraspecific trait variation in a mixed-species individual-based forest dynamics model – Part 2: Model evaluation for two Amazonian sites

Sylvain Schmitt[1,2,3], Fabian J. Fischer[4], James G. C. Ball[5], Nicolas Barbier[3], Marion Boisseaux[6], Damien Bonal[7], Benoit Burban[8], Xiuzhi Chen[9], Géraldine Derroire[10], Jeremy W. Lichstein[11], Daniela Nemetschek[4], Natalia Restrepo-Coupe[12], Scott Saleska[12], Giacomo Sellan[10], Philippe Verley[3], Gré goire Vincent[3], Camille Ziegler[6], Jérôme Chave[13], Isabelle Maréchaux[3]

[1]CIRAD, UPR Forêts et Sociétés, F-34398, Montpellier, France
[2]Forêts et Sociétés, Univ Montpellier, CIRAD, Montpellier, France
[3]AMAP, Univ Montpellier, INRAE, IRD, CIRAD, CNRS, F-34000 Montpellier, France
[4]School of Biological Sciences, University of Bristol, 24 Tyndall Avenue, Bristol, BS8 1TQ, UK
[5]Department of Plant Sciences, Downing Street, Cambridge, CB2 3EA, UK
[6]Univ. Bordeaux, INRAE, BIOGECO, 33612 Pessac, France
[7]Université de Lorraine, AgroParisTech, INRAE, UMR Silva, 54000 Nancy, France
[8]INRAE, UMR EcoFoG (Agroparistech, Cirad, CNRS, Université des Antilles, Université de la Guyane), Campus Agronomique, 97310 Kourou, French Guiana
[9]School of Atmospheric Sciences, Sun Yat-sen University, Guangzhou 510275, China
[10]Cirad, UMR EcoFoG (Agroparistech, CNRS, INRAE, Université des Antilles, Université de la Guyane), Campus Agronomique, 97310 Kourou, French Guiana
[11]Department of Biology, University of Florida, Gainesville, Florida 32611, USA
[15]University of Arizona, Ecology & Evolutionary Biology, Tucson, Arizona, United States of America
[13]Centre de Recherche Biodiversité et Environnement, UMR5300, CNRS, Université Paul Sabatier, IRD, INPT, Toulouse Cedex 9, France

Correspondence to: Sylvain Schmitt (sylvain.schmitt@cirad.fr)

All analyses are available here: https://sylvainschmitt.github.io/troll_eval/

Figures here: figures

Summary. We evaluate the capability of TROLL 4.0, a simulator of forest dynamics, to simulate tropical forest structure, diversity and functioning by comparing its outputs for two Amazonian forests with data of various nature. These include forest inventories, carbon and water fluxes between the forest and the atmosphere, and leaf area and canopy height from remote-sensing products. The model realistically predicts the structure and composition and the seasonality of carbon and water fluxes at both sites.

Abstract. TROLL 4.0 is an individual-based forest dynamics model that jointly simulates the structure, diversity and functioning of tropical forests, including their water balance, carbon fluxes and leaf phenology, while accounting for intraspecific trait variation for a large number of species. In a companion paper (Maréchaux et al., submitted companion paper), we describe how the model represents the physiological and demographic processes that control the tree life cycle in a metric-scale spatially-explicit scene and uses plant functional traits measurable in the field to parameterize such processes across species and individuals. Here we present a detailed evaluation of TROLL 4.0 for two Amazonian sites with contrasting soil and climate properties. We assessed the model's ability to represent forest structure and composition using lidar-derived canopy height distribution and forest inventories combined with information on species functional traits. We further evaluated the model's ability to represent carbon and water fluxes, as well as leaf area variation, at daily and fortnightly resolution over a decade, using detailed information from on-site eddy covariance towers, satellite data and ground-based or air-borne lidar data. We also compared the responses of carbon and water fluxes to environmental forcings between simulated and observed data. Overall, TROLL 4.0 provided a realistic representation of forests at both sites. The simulated canopy height distribution showed a high correlation coefficient with observed aerial and satellite data (CC>0.92), while the species and functional composition were well represented (CC>0.75). TROLL 4.0 also realistically simulated the seasonal variability of carbon and water fluxes (CC>0.46) and their responses to environmental drivers, while capturing temporal variations in leaf area (CC>0.76) and its partitioning in leaf age cohorts. However, TROLL overestimated annual gross primary productivity at both sites (mean RMSEP=0.94 kgC m^{-2} yr^{-1}) and evapotranspiration at one site (mean RMSEP=0.75 mm day^{-1}), likely due to an underestimation of the soil water depletion and stomatal control during the dry season. Overall, this evaluation highlights the potential of combining an integration of the processes underlying ecosystem fluxes with a representation of the structure and diversity of plant communities at a fine resolution. This could help predict the effects of a range of drivers on forest structure and dynamics, including climate change, fragmentation and forest management.

1 Introduction

Covering just 7% of the Earth's land surface, tropical forests play a disproportionately large role in the biosphere, storing around 25% of terrestrial carbon and contributing to more than a third of global terrestrial productivity (Bonan 2008). Regionally, tropical forests recycle around a third of precipitation through evapotranspiration, contributing to the generation and maintenance of a humid climate (Harper et al., 2013), effects that extend well beyond the tropics (Lawrence & Vandecar 2015). However the contribution of tropical forests to global biogeochemical cycles is threatened by ongoing deforestation, forest degradation and changes in climate and disturbances regimes (Lapola et al., 2023; Hubau et al., 2020; Qie et al., 2017), and tropical forests remain a major source of uncertainty in simulations of global biogeochemical cycles (Fisher et al., 2014; Koch et al., 2020).

In particular, many dynamic global vegetation models (DGVMs, Prentice et al., 2007) simulate a decrease in productivity with a seasonal decline in precipitation (Restrepo-Coupe et al., 2017, Chen et al., 2020), while observations from eddy-covariance data point to an increase in gross primary productivity during the dry season in light-limited tropical forests (Guan et al., 2015; Aguilos et al., 2018). Similarly, simulations of forest responses to experimental and natural droughts have highlighted large model-data discrepancies and variation across models (Powell et al., 2013; Joetzjer et al., 2014; Yao et al., 2023; Paschalis et al., 2022). Overall, improving models' representation of tropical forest functioning is an important research undertaking to foster our understanding and our ability to predict biogeochemical cycles.

To this end, a better integration of forest structure, diversity and functioning in models is needed (Purves and Pacala, 2008; McMahon et al., 2011; Evans, 2012; Mokany et al., 2016). Despite continuous advancements in this area (Fisher et al., 2018), such integration has been hindered by the coarse grained representation of vegetation in many models and subsequent difficulties to assimilate field data. Also, several processes driving the variation of tropical forest productivity and water fluxes remain poorly represented in vegetation models. These include water uptake by the root system and seasonal variation of leaf quantity and quality at the ecosystem-level, which are driven by leaf phenology and allocation processes at the individual-level (Chen et al., 2020; Wu et al., 2021; Restrepo-Coupe et al., 2017, Cusak et al., 2024).

A companion paper (Maréchaux et al., submitted companion paper), describes the individual-based forest dynamics model TROLL 4.0, which jointly simulates tropical forest structure, diversity and functioning, including forest water balance, carbon fluxes and leaf phenology, while accounting for intraspecific trait variation for a large number of species. TROLL 4.0 represents the processes underlying ecosystem fluxes, such as leaf gas exchanges and their responses to environmental variation, and is thus similar in this regard to DVGMs, with its outputs comparable with data from eddy covariance towers. However, unlike DGVMs that are designed for global applications and typically represent plant diversity with a few functional types, TROLL 4.0 represents diversity at the species level (e.g., 10s to 100s of tropical tree species). Furthermore, TROLL 4.0

is spatially-explicit and represents plant community structure and diversity at a metric-scale spatial resolution, which is consistent with that used by field ecologists. Physiological and demographic processes are integrated using a parameterisation based on plant traits measurable in the field, relying on recent knowledge in plant physiology and functional ecology. The individual-based, species-specific and spatially explicit representation of forest structure and composition enables TROLL 4.0 outputs to be directly compared with a range of data of different nature, including spatially explicit forest inventories, trait distribution or fine-scale remote sensing products.

In this paper, we evaluate TROLL 4.0 for two Amazonian sites with contrasting soil and climate properties. Specifically, we parameterized the model using functional trait and soil data at both sites. We first calibrated three major forest structure parameters using inventory data, and then the three parameters of the phenological module controlling leaf shedding as a function of soil water availability using litterfall data. We then evaluated the model's representation of forest structure and composition against independent data, including lidar-derived canopy height distribution, understory inventories and functional trait distribution. We further assessed the model ability to represent carbon and water fluxes, as well as leaf area variation, against eddy covariance, satellite and terrestrial or drone lidar data. We additionally compared the response of simulated and observed fluxes to incoming radiation, vapour pressure deficit, temperature, and wind speed. Our analyses establish the suitability of TROLL 4.0 for jointly simulating tropical forest structure, diversity and ecosystem functioning. Finally, we discuss the potential model-data discrepancies and identify priorities for future developments.

2 Methods

TROLL is an individual-based forest dynamics model. Individual trees are represented explicitly in an aboveground voxelized space (1 m^3), in which light transmission is modelled explicitly, and in a belowground space, in which water flows are simulated using a bucket model. The belowground space consists of several layers whose thickness and horizontal resolution (here 25 m^2) is user-defined. Each tree is labelled with a species associated with species-specific mean values for several plant traits provided as inputs, and is attributed individual trait values at recruitment as a function of trait variances and covariances, also provided as inputs. These traits determine the physiological and demographic processes that govern the life cycle of trees, from recruitment to growth, to seed dispersal, and finally death. Carbon assimilation by trees is computed using the photosynthesis model of Farquhar, von Caemmerer and Berry (1980), coupled to the stomatal conductance model of Medlyn et al. (2011), both as a function of the leaf micro-environmental conditions, tree access to water, and the leaf photosynthetic capacities and leaf respiration rate. The net carbon that remains after accounting for tree respiration is allocated to foliar production, carbon storage and tree woody growth following a hierarchical allocation scheme depending on the tree's environment and scaling relationships.

We conducted model calibration and evaluation at two lowland Amazon forest sites, the Paracou research station in French Guiana (5°28'N, 52°92'W), hereafter Paracou (Gourlet-Fleury et al., 2004; Bonal et al., 2008), and the Tapajos National Forest in Brazil in the K67 site also named BR-Sa1 (2°86'S, 54°96'W), hereafter Tapajos (Silver et al., 2000; Saleska et al., 2003). Both sites are covered by a high biomass and species rich tropical forest, and they present contrasting soil characteristics and climate (Table 1). The two sites have been intensively monitored for several decades, mainly through repeated forest inventories and eddy-flux tower measurements.

Specifically, at each site, we calibrated six global parameters, three parameters related to forest structure, and to which TROLL is known to be sensitive (the reference background mortality rate m, and the intercept a_{CR} and slope b_{CR} of the crown radius scaling relationship; Table S1; Maréchaux and Chave, 2017; Fischer et al., 2019), and the three parameters of the phenological module, new to TROLL 4.0 ($a_{T,o}$, $b_{T,o}$ and δ_o; Table S1). In TROLL 4.0, the shedding of old leaves is accelerated as soil water availability decreases (Maréchaux et al., submitted companion paper). Specifically, when the leaf predawn water potential (ψ_{pd}, MPa) falls below a threshold $\psi_{T,o}$ (MPa), the residence time of old leaves is decreased using a multiplicative factor f_0 <1. $\Psi_{T,o}$ varies with the tree leaf drought tolerance and its size as follows:

$$\psi_{T,o} = min(a_{T,o} \times \psi_{tlp}, -0.01 \times h - b_{T,o})$$

with ψ_{tlp}, the leaf water potential at turgor loss point in MPa, and h the tree height in m. f_0 is decremented (resp. incremented) by δ_o when $\psi_{pd} < \psi_{T,o}$ (resp. $\psi_{pd} > \psi_{T,o}$). $a_{T,o}$, $b_{T,o}$ and δ_o together control the intensity and timing of the peak of litterfall under drying soil conditions. While this scheme is process-based and relies on field observations as explained in Maréchaux et al. (submitted companion paper), uncertainties remain on the values of $a_{T,o}$, $b_{T,o}$ and δ_o that we therefore calibrated. After calibration, we then compared model outputs with site-specific data for evaluation at each site.

Table 1: Site overview with climate, vegetation and soil properties.

Variables	Units	Paracou	Tapajos	References
Climate				
Annual rainfall	mm	3,041	2,075	P: Aguilos et al., 2018; T: Silver et al., 2000
Average air temperature	°C	25.7	26.1	
Vegetation				
Aboveground carbon density ($DBH \geq 10$)	$Mg_C\ ha^{-1}$	209.5	143.7	P: Rutishauser et al., 2010; T: Rice et al., 2004

Abundance ($DBH \geq 10$)	ha^{-1}	612	470	P: Derroire et al., 2023; T: Rice et al., 2004
Basal area ($DBH \geq 10$)	$m^2\ ha^{-1}$	31	24	P: Derroire et al., 2023; T: Goncalves et al., 2018
Soil				
Type	-	Sandy clay loam	Clay	-
Depth	m	2.50	16.10	P: Hiltner et al., 2021; T: Nepstad et al., 2002
Layer thickness (top to bottom)	m	0.10 / 0.23 / 0.40 / 0.80 / 0.97	0.10 / 0.40 / 1.00 / 2.50 / 12.10	-
Sand	%	65.25	37.27	P: Van Langenhove et al., 2021; T: Silver et al., 2000
Clay	%	21.50	60.09	
Silt	%	13.25	2.64	
Soil Organic Content	%	2.37	2.54	P: Van Langenhove et al., 2021; T:Quesada et al., 2010
Dry Bulk Density	$g\ cm^{-3}$	1.040	1.125	P: Van Langenhove et al., 2021; T: Silver et al., 2000
Cation Exchange Capacity	$mEq\ 100g^{-1}$	2.98	2.97	P: Sabatier et al., 1997; T:Quesada et al., 2010
pH		4.34	3.84	P: Sabatier et al., 1997; T:Quesada et al., 2010

2.1 Simulation inputs and climatic drivers

TROLL 4.0 uses 35 global parameters defined by the user and provided as inputs. They relate to atmospheric constants, light diffusion, leaf carbon acquisition, leaf shedding, tree carbon allocation, tree shape, reproduction, and death, and intraspecific

trait variability (Table S1). Importantly, except the three parameters of forest structure mentioned above and the three parameters of the leaf shedding module that have been calibrated at each site, all values are common to the two sites.

TROLL 4.0 relies on a trait-based parameterization, which requires species-specific values of six functional traits and three scaling parameters to be provided as input. Scaling parameters include species maximum diameter at breast height (dbh_{max}, cm), and parameters defining the relationship between height and diameter at breast height (dbh), which are the asymptotic height (h_{lim}, m) and the parameter a_h (see Maréchaux et al. submitted companion paper, Eqs (16) and (62)). We used forest inventories from Paracou (Derroire et al., 2023) and Tapajos (Goncalves et al., 2018) to create a list of species present at each site, and computed dbh_{max} as the 95th quantile of species diameter at breast height for species including more than 10 individuals. We used the TALLO global database of height and diameter measurements (Jucker et al., 2022) to infer species-specific values of h_{lim} and a_h for the 496 species (24,609 trees with a mean of 49.62 ±730 trees per species) of the database that are present in Amazonia (latitude between 10°N and 18°S and longitude between 39°W and 78°W). Specifically, we inferred a_h and h_{lim} using Bayesian inference as follows:

$$log(h) \sim N[log(h_{lim} \times \frac{dbh}{a_h + dbh}), \sigma^2] \mid h_{lim} \sim N(h_{lim,0}, \sigma^2_h) \, , a_h \sim N(a_{h,0}, \sigma^2_a)$$

with the logarithm of height (h, in m) following a normal distribution centred on the log of a Michaelis-Menten model with asymptotic height $h_{lim,s}$, height-dbh scaling parameter $a_{h,s}$, and variance σ^2. The two species-specific parameters h_{lim} and a_h are random parameters following a normal distribution centred respectively on $h_{lim,0}$ and $a_{h,0}$ with variances σ^2_h and σ^2_a.

The functional traits used in the parameterization include unit leaf area (LA, in cm^2), leaf mass per area (LMA, $g.m^{-2}$), leaf nitrogen content per dry mass (N, $mg.g^{-1}$), leaf phosphorus content per dry mass (P, $mg.g^{-1}$), leaf water potential at turgor loss point (ψ_{tlp} , MPa), and wood specific gravity (wsg, $g.cm^{-3}$). We used the dataset provided by Vleminckx et al. (2021) combined with other published datasets (Boisseaux et al., submitted; Kattge, Bönisch, and al., 2020; Maréchaux et al., 2015; Maréchaux et al., 2019; Nemetschek et al., 2024; Ziegler et al., 2019) to retrieve species-specific mean values for these traits. Finally, we used predictive mean matching (Van Buuren and Groothuis-Oudshoorn, 2011) to impute missing trait values for a_h, h_{lim}, dbh_{max}, and ψ_{tlp} only. Overall, this leads to a parameterization of 114 species for Paracou and 113 species for Tapajos. These species pools are representative of the functional trait spaces of the two sites (Fig. S1).

The nine soil parameters of texture, depth and chemistry were gathered from the literature (Table 1), assuming a single soil type and depth per site for simplicity and setting the number of soil layers to five (Table 1). Testing the influence of horizontal and vertical soil heterogeneity on model outputs is left for future work.

TROLL 4.0 simulations are forced with six climatic drivers. Two of them are daily: cumulative rainfall (mm), and average nighttime temperature (°C). The remaining four drivers are provided every daytime half-hour: net radiation (S_{net}, $W.m^{-2}$), temperature (T, °C), vapour pressure deficit (VPD, kPa), and wind speed (WS, $m.s^{-1}$). Historical time series for these climatic variables have been retrieved from the FLUXNET 2015 dataset (Pastorello, Gilberto et al., 2020), which provides standardised data from eddy flux towers located at each site (2004-2014 for Paracou, and 2002-2011 for Tapajos). However, at Tapajos, rainfall data from FLUXNET 2015 is not reliable due to issues with rain gauges (Restrepo-Coupe et al., 2017). Instead we used rainfall data from the ERA5-Land reanalysis dataset (Muñoz-Sabater et al., 2021) available at hourly resolution between 2002 and 2011. Data from ERA5-Land for other climatic variables showed high correlation with FLUXNET 2015 data (not shown). We used spline interpolation to derive half-hourly time series from the hourly FLUXNET 2015 data in Tapajos. The half-hourly net radiation time series was used to define daytime hours (i.e. with $S_{net} > 0$) which were set from 6 a.m. to 6 p.m. in Paracou, and from 7 a.m. to 7 p.m. in Tapajos. The dry season was defined as a period with fortnightly rainfall below 50 mm on average across years, consistent with the 100 mm per month used by Bonal et al. (2008). This leads to a 4-month dry season in Paracou (August 1st to December 1st), and a 4.5-month dry season in Tapajos (June 15 to November 1st). Dry seasons were defined for illustration purposes only and have no effect on the model behaviour, which is driven by the meteorological inputs described above.

2.2 Simulation set-up and calibration

We calibrated the three forest structure parameters (m, a_{CR} and b_{CR}) for each site. a_{CR} and b_{CR} are not independent, and we used the TALLO global database of crown radius (CR) and diameter (dbh) measurements (Jucker et al., 2022) to infer their relationship. To do so, we restricted the TALLO database to observations located 10-km around sites from which we generate a thousand pairs of (a_{CR}, b_{CR}) values. Each pair of values was determined by randomly drawing 10 individuals per 10-cm diameter classes to generate a size-balanced dataset to which the following model was fitted: $log(CR) \sim N[a_{CR} + b_{CR} \times log(dbh), \sigma^2]$. This resulted in the following linear relationship between the two parameters: $b_{CR} = -0.39 + 0.59 \times a_{CR} + \epsilon_{b_{CR}}$, with $\epsilon_{b_{CR}}$ the error around the relation. This relationship constrained the exploration of the three-dimensional parameter space, and we actually calibrated a_{CR}, $\epsilon_{b_{CR}}$, and m. Based on preliminary exploratory analyses with the previous version of TROLL, we defined the range of calibration for each parameter and site as follows: a_{CR} varied from 1.60 to 2.00 in Paracou and from 2.3 to 2.7 in Tapajos with a step of 0.05, $\epsilon_{b_{CR}}$ from -0.30 to 0.10 in both sites with a step of 0.05, and m from 0.030 to 0.050 in both sites with a step of 0.0025. This resulted in $9\ a_{CR} \times 5\ \epsilon_{b_{CR}} \times 9\ m \times 2\ site = 810$ triplets of parameter values.

For each set of three parameter values, we performed a 4-ha 600-year simulation from bare ground with TROLL 4.0. Simulations were run with an external seed rain uniformly distributed across species, so that the simulated community structure is an emergent property resulting from the community assembly mechanisms embedded in the model. As succession unfolds

and the number of mature trees increases in the simulation, the production of seeds by the simulated trees progressively increases. An alternative to uniform seed rain across species would be to prescribe non-uniform seed rain based on species' regional abundances. This approach would tend to make the simulated species abundances resemble the observed regional abundances. In contrast, our approach (uniform seed rain) biases the simulated abundances towards evenness across species, and we can therefore be confident that differences in simulated abundances reflect differences in demographic performance controlled by the model trait-based parameterization rather than differences in prescribed seed rain. Each simulation was forced each year by randomly drawing a year among the ten years of climatic data. In doing so, we avoided applying a periodic climatic forcing or any potential trend linked to global warming. For both sites, simulations were performed with $a_{T,o}$=0.2, $b_{T,o}$ =0.02, and δ_o =0.2 as a priori values.

To evaluate the forest structure simulated with each triplet of parameter values in Paracou, we compared simulated total basal area (BA^{tot}, $m^2.ha^{-1}$), total tree abundance (N^{tot}, ha^{-1}), and tree abundances per 5-cm diameter class (N^{dbh}, ha^{-1}) at the end of the 600-year regeneration to a 2015 inventory of trees with dbh >10 cm in six 6-ha plots (Derroire et al., 2023). To evaluate the forest structure simulated with each triplet of parameter values in Tapajos, we compared simulated total aboveground biomass (AGB^{tot}, $Mg_C.ha^{-1}$), total tree abundance (N^{tot},ha^{-1}), and tree abundances per 5-cm diameter class (N^{dbh}, ha^{-1}) at the end of the 600-year regeneration to a 1999 inventory of trees with dbh > 10 cm in 19.75 ha along four 1-km transects in Tapajos (Rice et al., 2004). For each simulation we calculated the relative root mean squared error defined as:

$$RRMSEP = \frac{X_o^{tot} - X_s^{tot}}{X_o^{tot}} + \frac{N_o^{tot} - N_s^{tot}}{N_o^{tot}} + \frac{\sqrt{\frac{1}{N_{dbh}} \times \sum_{dbh=10}^{dbh=200} (N_o^{dbh} - N_s^{dbh})^2}}{|N_o^{dbh}|}$$

where X^{tot}_o, N^{tot}_o and N^{dbh}_o are observed values, and X^{tot}_s, N^{tot}_s and N^{dbh}_s are the simulated values, X being BA in Paracou and AGB in Tapajos. We extracted the simulation with the lowest *RRMSEP* at each site and used the corresponding values for *m*, a_{CR} and b_{CR} in all subsequent simulations.

This 600-year simulation resulted in mature forests with stable forest structure, composition, and functioning in both sites. Starting from this stable end-state, we then performed simulations to calibrate the three parameters of the phenological module. Specifically, we used all the combinations of $a_{T,o}$ in [0.01, 0.025, 0.05, 0.075, 0.1, 0.2, 0.3, 0.4, 0.5], $b_{T,o}$ in [0.01, 0.015, 0.02, 0.05, 0.04, 0.06, 0.08, 0.10], and δ_o in [0.1, 0.2, 0.3, 0.4, 0.5] resulting in 9 $a_{T,o}$ × 8 $b_{T,o}$ × 5 δ_o × 2 $sites$ = 720 simulations. For each triplet of values, we ran a 20-year simulation with historical weather starting from the 600-year regeneration end state. Only the last 10 years were used for the calibration itself to allow the leaf dynamics to adjust to new parameter values.

To evaluate each simulation, we used leaf litter data from litter traps at both sites (D. Bonal & B. Burban pers. com. and Rice et al., 2008). Litter traps were collected fortnightly most of the time (although time intervals between consecutive litter trap

collections were sometimes higher and up to 80 days in Paracou) between 2004 and 2023 in Paracou, and between 2000 and 2005 in Tapajos. Trap content was oven-dried until stable weight, partitioned between leaves, fruits and woody debris, and weighted. We computed observed leaf litterfall flux in $Mg.ha^{-1}.year^{-1}$ as the mean across traps converted from trap surface to hectare and time interval in days to year. We also recorded the time interval between consecutive trap collections to account for the smoothing effect of the longer time intervals. Simulated leaf litterfall fluxes over the last 10 years of simulation for each triplet of parameter values were compared to the observed fluxes using the same observation dates and corresponding time intervals.

To compare simulations against observations, we defined two yearly indices that quantify the timing and intensity of the litterfall peak. Both indices are influenced by the three parameters in simulations and are key features of litterfall patterns in tropical rainforests (Chave et al., 2010; Yang et al., 2021). The two indices are (i) the day of the litterfall peak as the Julian day of the maximum annual litterfall flux value (*day*), and (ii) the ratio between the maximum value (computed as the average of litterfall flux over the two consecutive time intervals before and after the peak day) divided by the basal flux (computed as the average between January and April) (*ratio*). For each simulation we then calculated the root mean squared error defined as:

$$RMSEP = \sqrt{\frac{\sum_{y=y_0}^{y=y_{max}} (ratio_{y,o} - ratio_{y,s})^2}{N_{year}} + \frac{\sum_{y=y_0}^{y=y_{max}} (day_{y,o} - day_{y,s})^2}{N_{year}}}$$

where $day_{y,o}$ and $ratio_{y,o}$ are the reduced centred indices computed for year y with the observations, and $day_{y,s}$ and $ratio_{y,s}$ are the reduced centred indices computed for year y with the simulations. Thus a R*MSEP* of 1 corresponds to a ratio error of one standard deviation, *i.e.* 7.6 folds, or to a day error of one standard deviation, *i.e.* 45.5 days. The best-fit parameters were those corresponding to the lowest *RMSEP* at each site.

Finally, we ran ten replicates of 10-year simulations with historical weather and starting from the end state of the selected calibration simulation to quantify the envelopes of simulation outputs. In the future, assessment of the model stochasticity on forest structure and composition should be made by replicating the initial 600-years spin-up simulations. All simulations were run using TROLL 4.0 (Maréchaux et al., submitted companion paper) wrapped in the R package *rcontroll* (Schmitt et al., 2023) and encapsulated in a Singularity image (Kurtzer et al., 2017) leveraging a Python Snakemake workflow (Köster et al., 2012) in a high performance computing platform using 100 cores.

2.3 Evaluation of forest structure and composition

To assess the model's ability to simulate forest structure, species and functional composition, we used airborne lidar scanning (ALS) and satellite data, as well as forest inventories combined with functional traits. We evaluated the diameter distribution of the forest understory at Paracou using a 9-ha inventory of trees with dbh between 1 and 10 cm from 2020-2023 (Sellan,

Derroire, Chave unpublished). We evaluated the structure of the final simulated forest against observed basal area (BA, $m^2.ha^{-1}$) and logarithm of tree abundance (ha^{-1}) per 1-cm diameter class below 10 cm. We evaluated tree height distributions using ALS data from 2015 at Paracou (Vincent unpublished) and from 2012 at Tapajos (dos-Santos et al., 2019), which we processed into canopy height models with a standardised pipeline (Fischer et al., 2024). We also compared the simulated tree height distributions with a canopy height model from the Global Ecosystem Dynamics Investigation instrument at both sites (Eegholm et al., 2019). We evaluated the species composition of the final simulated forest against the observed rank-abundance curve of the 114 most abundant species at both sites. Finally, we evaluated the functional composition of the final simulated forest against the observed density distribution of each trait for each site and each plot. Due to a lower taxonomic resolution of botanical identification at the Tapajos site, we used genus level functional trait data in Tapajos and species level functional trait data in Paracou.

2.4 Evaluation of leaf area dynamics

We assessed the model's ability to represent the dynamics of total leaf area and its partitioning into three leaf age cohorts (see Maréchaux et al., submitted companion paper). For evaluation, we gathered multiple datasets of leaf area index (LAI): LAI from MODIS satellites at both sites, LAI from terrestrial lidar in Tapajos (Smith et al., 2019), LAI from UAV-borne lidar in Paracou (Barbier, Verley, Vincent, unpublished; Vincent et al., 2017). MODIS LAI was measured at resolutions of 8 days and 500 m and pre-processed in PLUMBER2 (Ukkoloa et al., 2020) for each site with the corresponding time periods. At Tapajos, plant area index (PAI) was derived from terrestrial lidar scanning performed every 1-2 months in 2010, 2012, 2015 and 2017 over 0.4-ha by moving a vertical lidar sensor along four 1-km long transects with a spatial resolution of about 3 m to characterise canopy porosity (Smith et al., 2019). PAI was derived from lidar hits following Stark et al. (2012) and using the MacArthur–Horn transformation (MacArthur & Horn, 1969). This PAI was further adjusted into LAI using the annual mean LAI of 5.7 (Stark et al., 2012). In Paracou, the PAI was derived from UAV-borne lidar resulting in a PAI with resolutions of 21 days and 1 m between 2020 and 2022 over 2.5 hectares. This PAI derived from UAV lidar was obtained by vertical integration of Plant Area Density (PAD) profiles previously recalibrated to match a TLS-derived PAD profile of a common 1-ha plot scanned in October 2019. This was required because the limited penetration of the UAV lidar yielded large overestimation of raw PAD values (Vincent et al., 2023). This PAI was further rescaled into LAI variation with a factor of 0.68 for comparisons with LAI variations from other products. By comparison, TROLL simulates daily LAI at 1 m resolution.

Simulated LAI variations per leaf age cohort (see Eqs (56)-(57) in Maréchaux et al. submitted companion paper) were compared qualitatively against the one derived from phenological cameras by Wu et al., (2016) in Tapajos and from the reanalysis of Yang et al. (2023) at both sites. Wu et al. (2016) used 478 images spread over 24 months and 65 trees and fitted the transition from young to mature and from mature to old leaf pools at 1 and 3 months, respectively. Yang et al. (2023) used satellite observations of TROPOMI sun-induced chlorophyll fluorescence as an indicator of leaf photosynthesis variation, validated by multiple *in situ* measurements, and set the transition from young to mature and from mature to old leaf pools at

1.71 and 5.14 months respectively. By comparison, leaf age per cohort depends on the individual leaf lifespan in TROLL 4.0 (see Maréchaux et al. submitted companion paper).

2.5 Evaluation of carbon and water fluxes

To assess the model's ability to simulate carbon and water fluxes, we focused respectively on gross primary productivity (GPP, $kg.m^{-2}.yr^{-1}$) and evapotranspiration (ET, $mm.day^{-1}$). We extracted GPP and latent heat flux (LE, $W.m^{-2}.half-hour^{-1}$) from the FLUXNET 2015 dataset (Pastorello, Gilberto et al., 2020). ET was derived from LE and temperature (T, in °C) using $ET = \frac{LE \times 60 \times 30 \times 10^{-6}}{\lambda(T)}$ $with$ $\lambda(T) = 2.501 - (2.361 \times 10^{-3}) \times T$. We additionally derived potential evapotranspiration estimated with the Penman–Monteith equation. We summarised half-hourly GPP and ET into daily values by calculating respectively the daily mean and sum. TROLL 4.0 carbon fluxes were also compared with a remotely sensed product of GPP derived from Solar Induced Fluorescence (SIF) from TROPOMI satellite instruments using the formula $GPP = 15.343 \times SIF$ (Chen et al. 2022). We further compared how the fluxes depended on environmental drivers in both simulated and observed data. Using the FLUXNET 2015 dataset (Pastorello, Gilberto et al., 2020), daily values of cumulative photosynthetically active radiation (PAR, $mol.m^{-2}$), maximum vapour pressure deficit (VPD, kPa), mean temperature (T, $°C$), and mean wind speed (WS, $m.s^{-1}$) were calculated, and simulated and observed responses of GPP and ET to PAR, VPD, T and WS were compared. We additionally assessed TROLL 4.0 water fluxes using the relative variation of soil water content (RSWC, %) from the top horizon (soil depth up to 10 cm) from Paracou eddy flux tower (Bonal et al., 2008), defined as the daily mean value of soil water content ($m^3.m^{-3}$) divided by the yearly 95th quantile of daily mean.

3 Results

3.1 Forest structure and composition

Calibration of background mortality rate (m) and crown radius scaling parameters (a_{CR} and b_{CR}) at Paracou and Tapajos against observed basal area or aboveground biomass, total abundance and abundance per 5-cm dbh classes resulted in m=0.035, a_{CR}=1.80 and b_{CR}=0.3860 at Paracou, and m=0.040, a_{CR}=2.45 and b_{CR}=0.7565 at Tapajos. The corresponding basal area or aboveground biomass, total abundance and abundance per 5-cm dbh classes are in very good agreement with observations (CC>0.99 in both sites, Fig. 1). The three parameter values were very similar across the five best simulations (m±0.0025, a_{CR}±0.1 and b_{CR}±0.057 at Paracou and m±0.01, a_{CR}±0.1 and b_{CR}±0.0285 at Tapajos), and we used the values of the best simulation in all subsequent analyses.

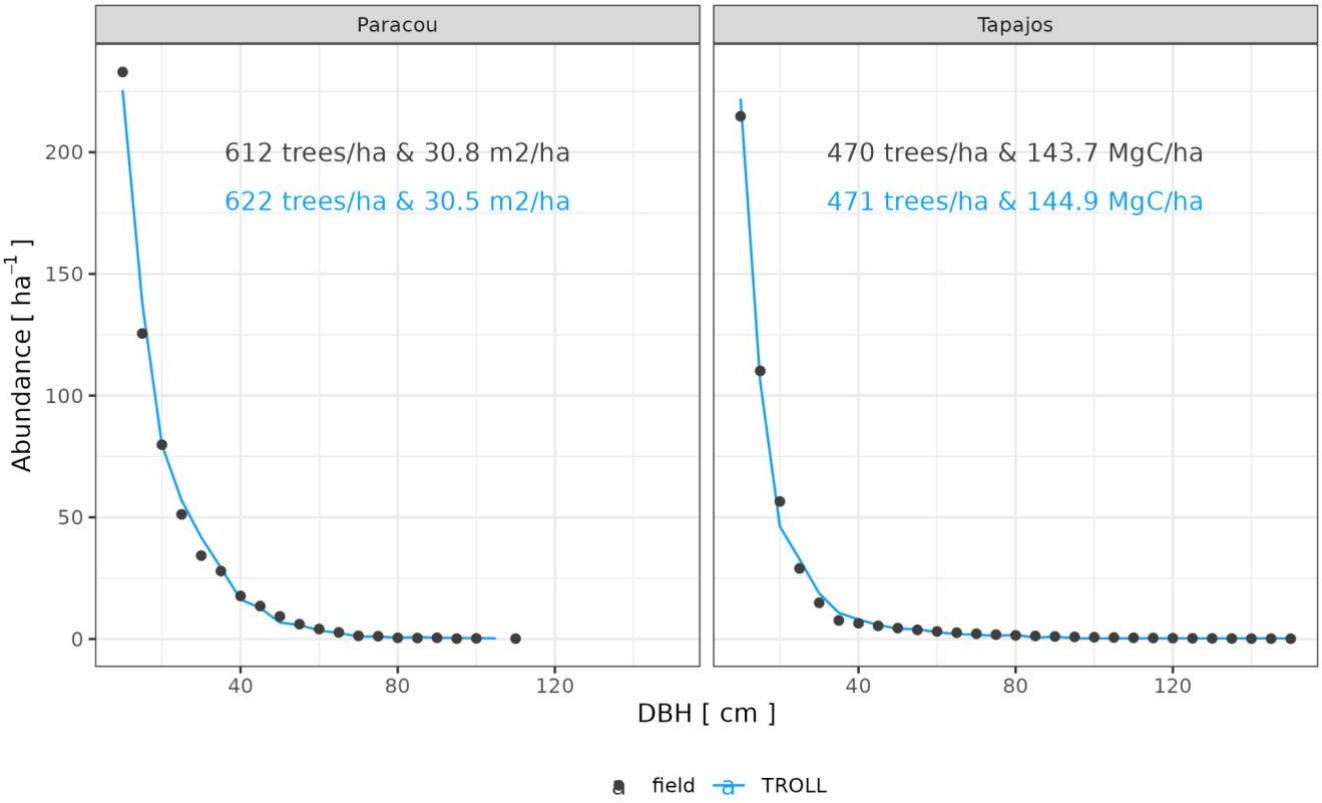

Figure 1: Tree size structure at Paracou and Tapajos, expressed in terms of tree abundances per 5 cm-dbh classes. Comparison between distributions simulated by TROLL 4.0 after calibration of m, a_{CR} and b_{CR} in blue and the ones derived from field inventories of trees with dbh >10 cm in black, at Paracou (left) and Tapajos (right). Observed (black) and simulated (blue) densities of trees with dbh > 10 cm, and basal area (for Paracou) or aboveground biomass (for Tapajos) are also provided. All simulated values correspond to the end-state of a 600-year regeneration from bare soil with calibrated values for m, a_{CR} and b_{CR} at each site.

After calibration, the height distribution simulated by TROLL 4.0 corresponded very well to that measured by lidar aerial scanning (ALS) or lidar satellite scanning (GEDI), with a root mean square error of prediction (RMSEP) below 0.8% and a correlation coefficient (CC) above 0.91, despite a slight overestimation of understory density in Paracou at heights below 20 m and a slight underestimation of overstory density above 40 m in Tapajos, in comparison to ALS but not GEDI. TROLL 4.0 simulations also reproduced the forest understory structure characterised by basal area (BA) and tree abundance distribution per 1-cm diameter classes for trees < 10 cm dbh at Paracou (Fig. 3). TROLL 4.0 underestimated the number of small trees (2,139 vs. 3,787 trees ha^{-1}), resulting in an underestimated BA (2.9 vs. 3.7 $m^2.ha^{-1}$).

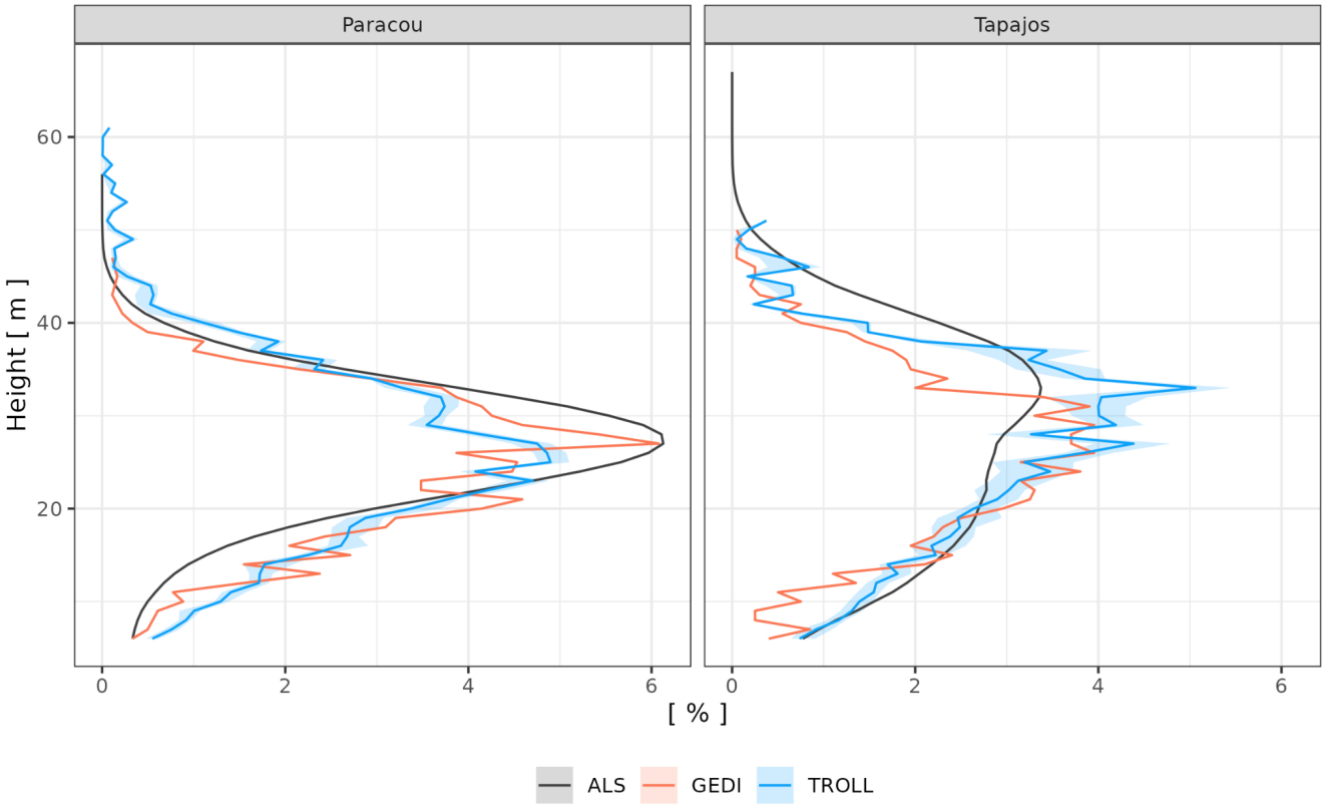

Figure 2: Canopy height distribution at Paracou and Tapajos, expressed in terms of proportion (%) of pixels per 1-m height classes. Comparison between distributions derived from a canopy height model simulated by TROLL 4.0 (blue lines), the ones derived from a canopy height model from airborne laser scanning (black lines), and the ones derived from a canopy height model from the Global Ecosystem Dynamics Investigation instrument (red lines). Simulated values correspond to the end-state of simulations of 600-year regeneration from bare ground and the confidence intervals were estimated generating an ensemble of 10 10-year simulations for each site (see methods).

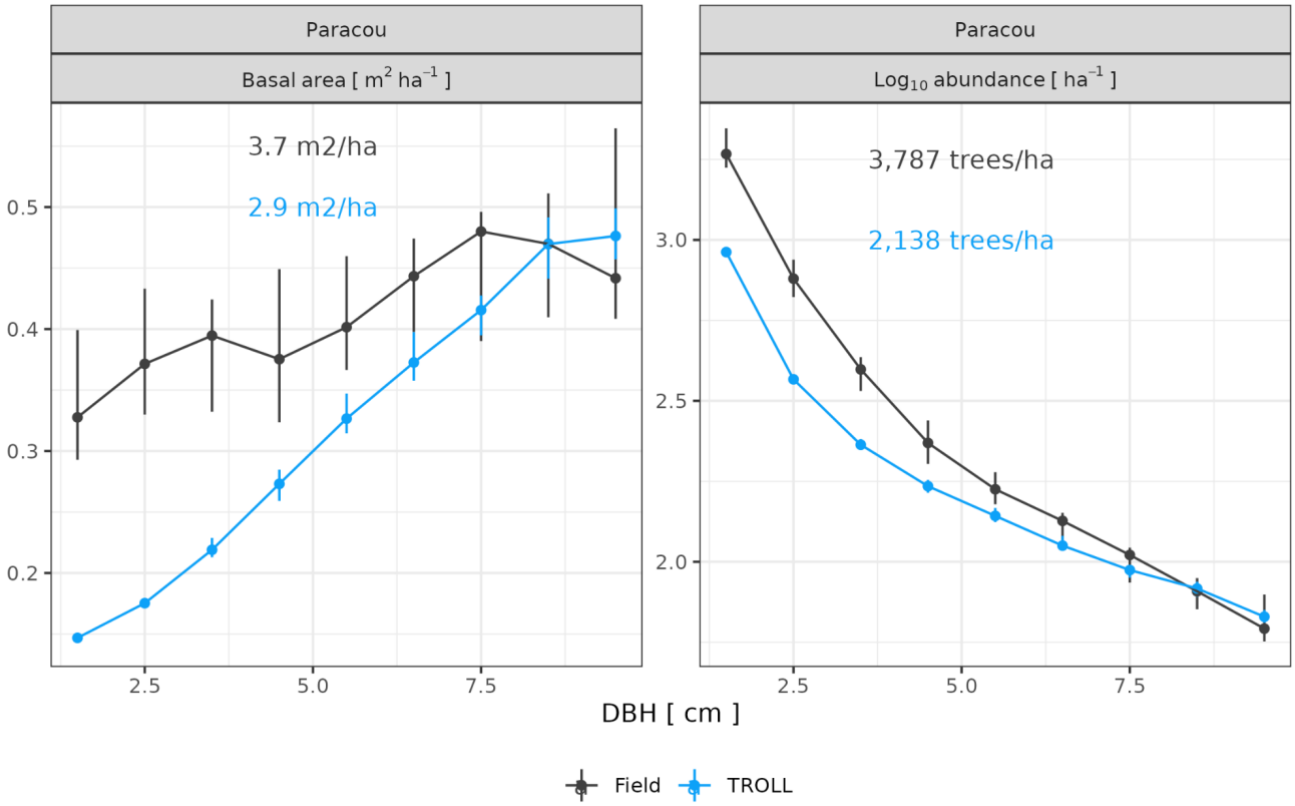

Figure 3: Understory tree size structure at Paracou, expressed in terms of basal area distributions (left) and tree abundance (right) per 1 cm-dbh classes. Comparison between distributions simulated by TROLL 4.0 in blue and the ones derived from field inventories of trees with dbh >1 cm and < 10 cm in black. Simulated values correspond to the end-state of simulations of 600-year regeneration from bare ground. Confidence intervals at 95 % are shown with error bars and are based on variations among plots (9 plots of 1 ha) for the observations. The confidence intervals for simulated values was estimated generating an ensemble of 10 10-year simulations (see methods). Simulated (blue) and observed (black) total basal area (left) and densities (right) for trees with dbh >1 cm and < 10 cm are also provided.

At Paracou, the simulated and observed rank-abundance curves were similar (Fig. 4), with a RMSEP of 3.67 trees.ha^{-1} and a CC of 0.93, but with an underestimation in the abundance of dominant species and an overestimation in the abundance of rare species resulting in a higher evenness overall. At Tapajos, the simulated and observed rank-abundance curves displayed similar patterns as at Paracou but amplified (RMSEP=3.62 trees.ha^{-1} and CC=0.94), with a strong underestimation of the abundance of dominant species and an overestimation of the abundance of rare species.

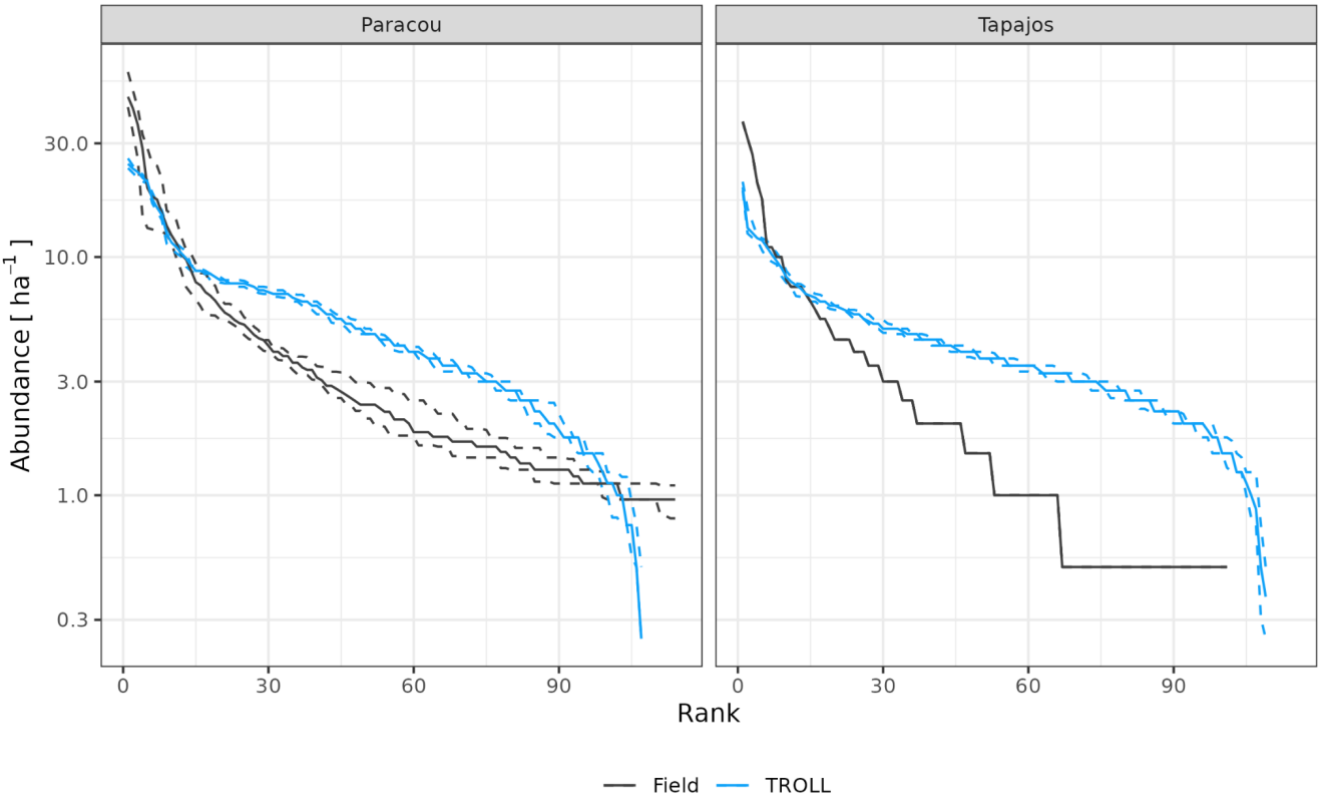

Figure 4: Species-rank abundance curves at Paracou and Tapajos. Comparisons between curves simulated by TROLL 4.0 (blue) and derived from field inventories at both sites. Simulations included 114 and 113 species at Paracou and Tapajos respectively. Curves derived from inventories were cut at the 114th species. Simulated values correspond to the end-state of 600-year regeneration from bare ground. Confidence intervals at 95 % are shown with error bars and are based on variations among plots for observations. The confidence interval for the simulated values was estimated generating an ensemble of 10 10-year simulations (see methods).

Functional trait distributions simulated by TROLL 4.0 were consistent with empirical ones at Paracou and Tapajos (Fig. 5), with a CC from 0.91 to 1.00 for all traits at both sites, except for leaf area at Paracou (CC=0.74) and Tapajos (CC=0.87). Abundances of low wood density trees, high LA trees, and high LMA trees were underestimated in simulations in comparison to observations at Paracou however.

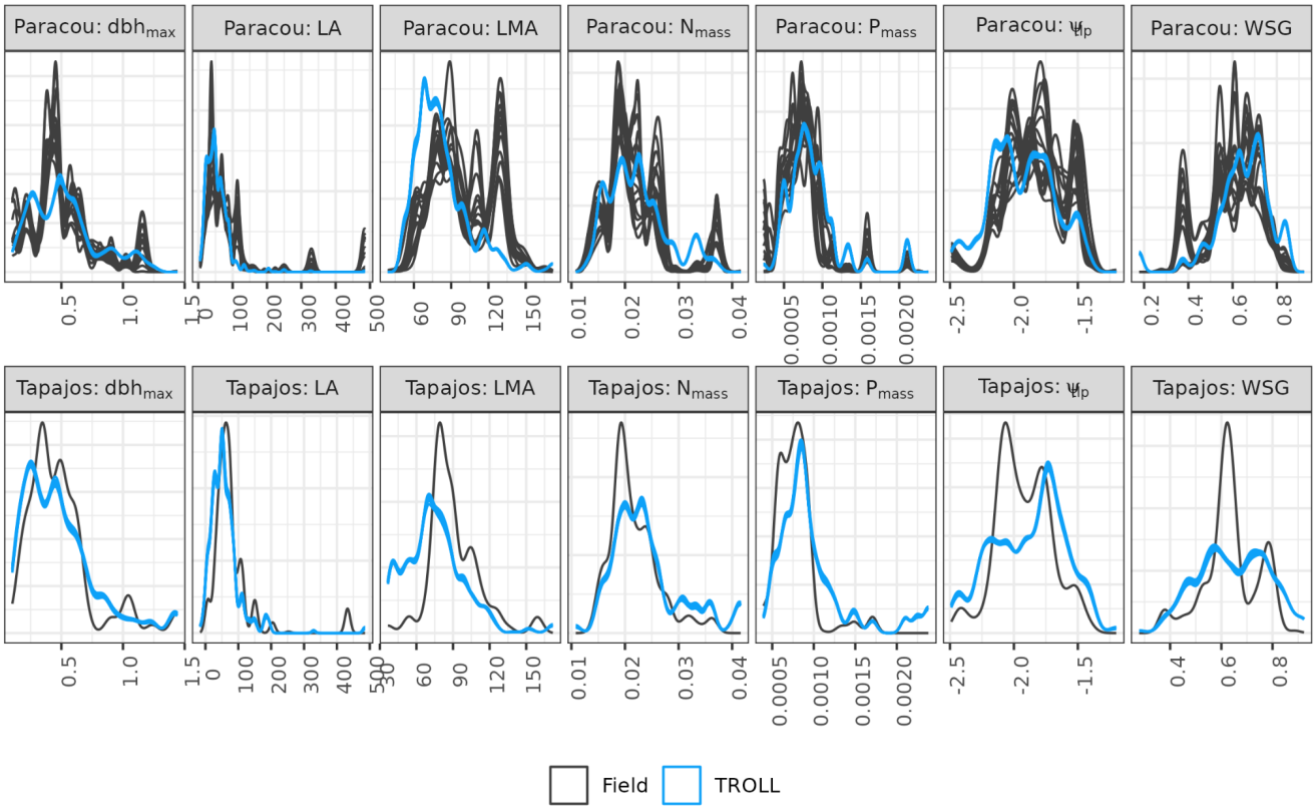

Figure 5: Functional trait distributions at Paracou and Tapajos. Distributions derived from field inventories (black) were based on botanical identification at the species level in Paracou and the genus level in Tapajos. Simulated distributions (blue) were based on the final stage of one 4-ha 600-year regeneration from bare soil. Confidence intervals are shown with repeated lines and are based on variations among plots for observations. dbh_{max}: maximum diameter in m, LA: leaf area in cm^{-2}, LMA: leaf mass per area in $g\ cm^{-3}$, N_{mass}: leaf nitrogen content per dry mass in $mg\ g^{-1}$, P_{mass}: leaf phosphorus content per dry mass in $mg\ g^{-1}$, Ψ_{tlp}: leaf water potential at turgor loss point in MPa, WSG: wood specific gravity in $g\ cm^{-3}$.

3.2 Leaf phenology

The calibration of the new leaf shedding module against observed litterfall at Paracou and Tapajos illustrated how each parameter affected the simulated timing and intensity of the litterfall peak during the dry season (Fig. S2). Calibration resulted in a best-fit $a_{T,o}$ value of 0.2, and a $b_{T,o}$ value of 0.015 at both sites. The calibrated δ_o differed across sites (δ_o=0.1 at Paracou and δ_o=0.2 at Tapajos). The resulting simulated seasonal variation of litterfall at Paracou and Tapajos (Fig. 6) is qualitatively in good agreement with observations. Both empirical and simulated data showed a marked peak in litterfall during the dry season, despite a clear under-estimation of simulated litterfall flux during the wet season, particularly at Tapajos, and a delayed peak during the dry season, particularly at Paracou, in comparison to observations.

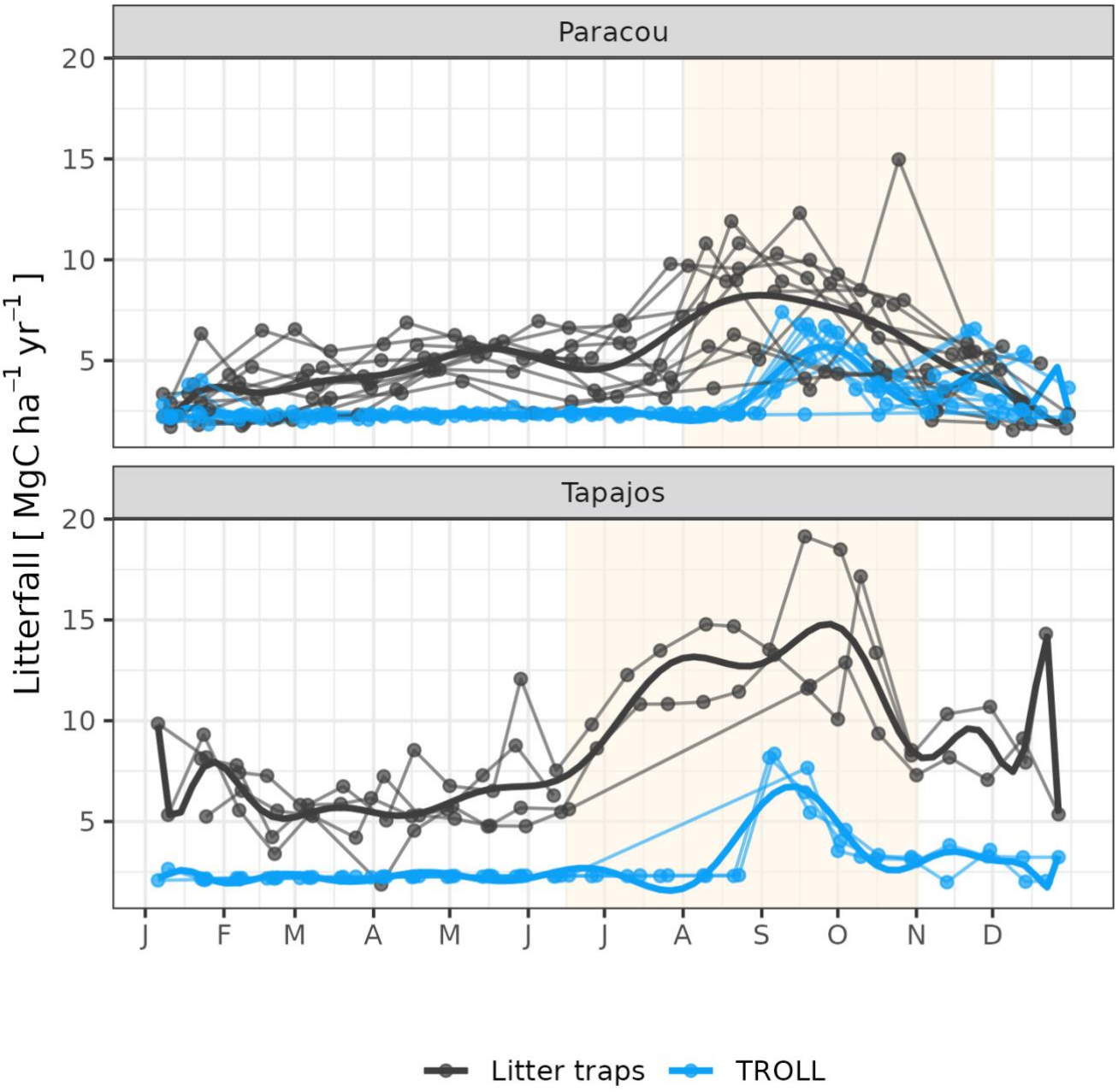

Figure 6: Litterfall annual cycle from fortnightly litterfall fluxes at Paracou and Tapajos. Each thin line represents one year with points showing values at sampling dates, the thick lines represent polynomial smoothing among years, and the vertical yellow bands in the background correspond to the site's climatological dry season. Simulated values correspond to the last 10 years of 20-year simulations starting from the end-state of 600-year regeneration from bare soil with calibrated parameters at each site.

The empirical LAI datasets displayed strikingly different results, illustrating the challenge of robustly estimating LAI in dense tropical forests (Fig. 7, Tab. S2). MODIS-derived LAI displayed almost no seasonality with values around 6 $m^2.m^{-2}$ at both sites. At Paracou LAI derived from UAV-borne lidar showed a clear seasonality, with lowest values around 5.5 $m^2.m^{-2}$ from April to June and highest values of almost 6 $m^2.m^{-2}$ in December, at the end of the dry season. At Tapajos, LAI derived from terrestrial lidar showed no seasonality, and stayed around 5.75 $m^2.m^{-2}$ throughout the year, but LAI derived from phenological cameras (PhenoCams) was seasonal, with lowest values at 5.5 $m^2.m^{-2}$ in June and highest values above 6 $m^2.m^{-2}$ in December, at the end of the dry season. These observations were compared with simulations. At Paracou, simulated LAI matched the one derived from UAV-borne lidar, both showing an increase during the dry season (CC=0.84, RMSEP=0.11 $m^2.m^{-2}$). At Tapajos, simulated LAI matched the empirical LAI derived from PhenoCams (CC=0.91, RMSEP=0.15 $m^2.m^{-2}$; Table S2).

The different datasets we gathered to estimate LAI dynamics per cohorts also showed contrasted patterns (Fig. 8 and Fig. S3). At Tapajos, PhenoCams indicate a maximum young leaf LAI reached during the dry season and a minimum during the wet season, with inverse patterns for old leaf LAI. TROLL 4.0 simulations yielded patterns consistent with these observations (Fig. 8). However, Yang et al.'s (2023) reanalysis predicts exactly opposite trends for young and old leaves, with a maximum young leaf LAI during the wet season and a minimum during the dry season. At Paracou, we could only compare simulated trends against Yang et al. (2023)'s reanalysis showing a relatively poor match (Fig 8).

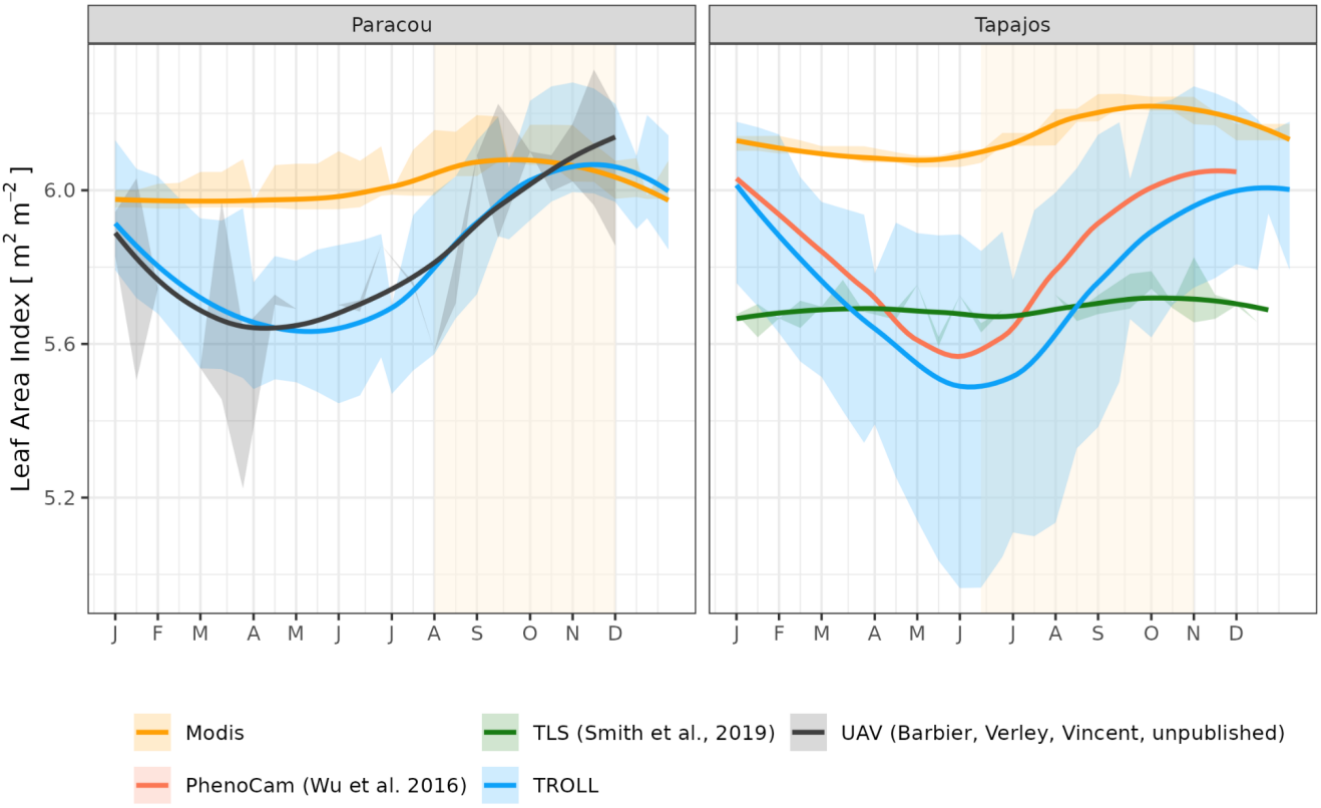

Figure 7: Mean annual cycle of leaf area index (LAI) for Paracou and Tapajos, derived from fortnightly means, from different sources (see methods). Bands are the intervals of means across years, and the vertical yellow bands in the background correspond to the site's climatological dry season. Simulated values correspond to 10 years of simulations starting from the end-state of 600-year regeneration from bare soil with calibrated parameters at each site.

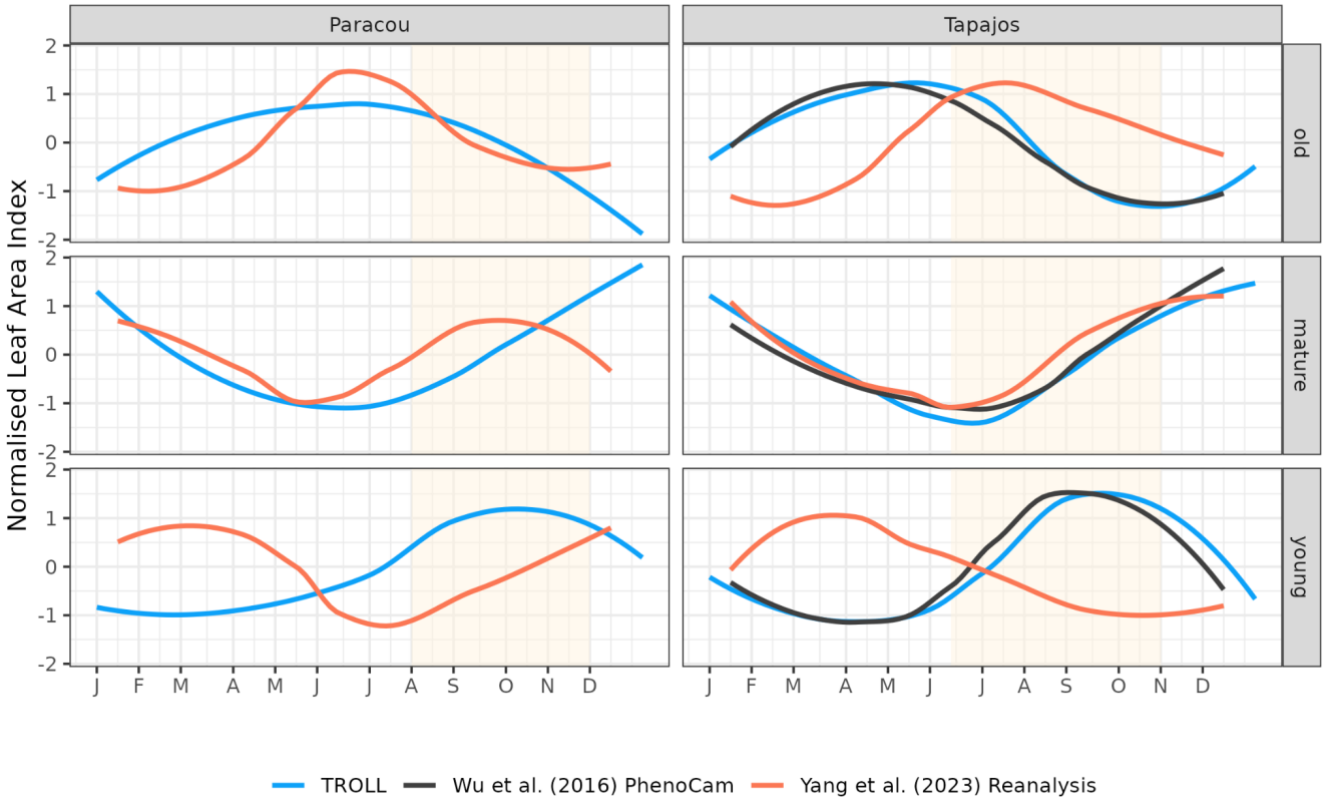

Figure 8: Mean annual cycle of normalised leaf area index per leaf age cohorts, derived from fortnightly means, at Paracou and Tapajos. Note that the three leaf age cohorts (young, mature and old leaves) are not defined the same way in the three sources. Leaf age per cohort depends on the individual leaf lifespan in TROLL 4.0 (see Maréchaux et al., submitted companion paper), while the transition from young to mature and mature to old are respectively fixed to 1.71 and 5.14 months in Yang et al. (2023) and fitted to 1 and 3 months in Wu et al. (2016). The vertical yellow bands in the background correspond to the site's climatological dry season. See figure S3 for absolute variation per cohort, site and dataset. Simulated values correspond to 10 years of simulations starting from the end-state of 600-year regeneration from bare soil with calibrated parameters at each site.

3.3 Water and carbon fluxes

TROLL 4.0 captured the seasonality of gross primary productivity (GPP) observed at the two sites, with an increase before the onset of the dry season, reaching its maximum during the dry season, and a decrease starting before or at the onset of the wet season (Fig. 9 and see Fig. S4 for interannual variations, Tab. S2), leading to a CC of 0.60 and 0.46 when compared to eddy-flux estimates at Paracou and Tapajos respectively. TROLL 4.0 consistently overestimated GPP at both sites, particularly during the dry season, with a RMSEP of 0.75 and 1.12 $kgC_{\square}\, m^{\square^{-2}}\, yr^{\square^{-1}}$ when compared with eddy-flux estimates at Paracou and Tapajos, respectively. GPP estimates from TROPOMI SIF were systematically lower than the eddy-flux estimates, which were themselves systematically lower than the TROLL 4.0 simulations.

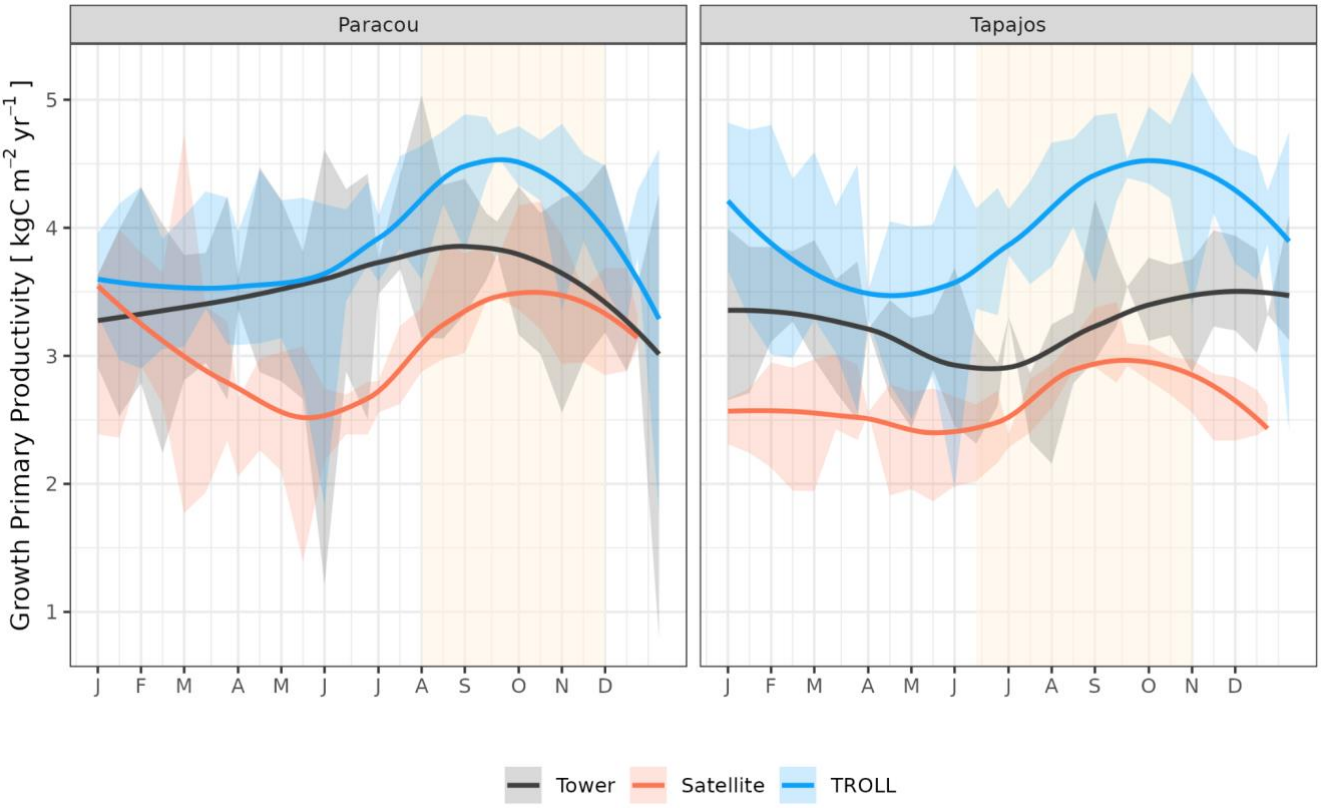

Figure 9: Mean annual cycle of gross primary productivity for Paracou and Tapajos, derived from fortnightly means. The red lines represent the gross primary productivity estimated from TROPOMI SIF while the black lines represent the one derived from eddy-flux measurements, and the blue lines the simulated gross primary productivity with TROLL 4.0. Bands are the intervals of means across ten years, and the vertical yellow bands in the background correspond to the site's climatological dry season. Simulated values correspond to 10 years of simulations starting from the end-state of 600-year regeneration from bare soil with calibrated parameters at each site. Inter-annual variations are shown in Figure S4.

The seasonality of water flux was captured by TROLL 4.0 (Fig. 10 and see Fig. S5 for interannual variations, Tab. S2), with a pronounced increase in evapotranspiration (ET) during the dry season at both sites, and leading to CC of 0.66 and 0.70 when compared with eddy-flux estimates at Tapajos and Paracou respectively. Although intra-annual variations of simulated and observed values overlapped, TROLL 4.0 tended to overestimate ET in Tapajos during the dry season while staying under the potential evapotranspiration, leading to RMSEP values of 0.60 and 0.75 $mm.day^{-1}$ when compared with eddy-flux estimates at Paracou and Tapajos respectively. TROLL 4.0 also captured the seasonality in RSWC of the top soil layer at Paracou (Fig. S6, Table S2, see Fig. S7 for absolute variation with varying depth), with a high RSWC in the wet season close to 100% and a sharp decrease in RSWC in the dry season, although smoother in simulations than field estimates on average.

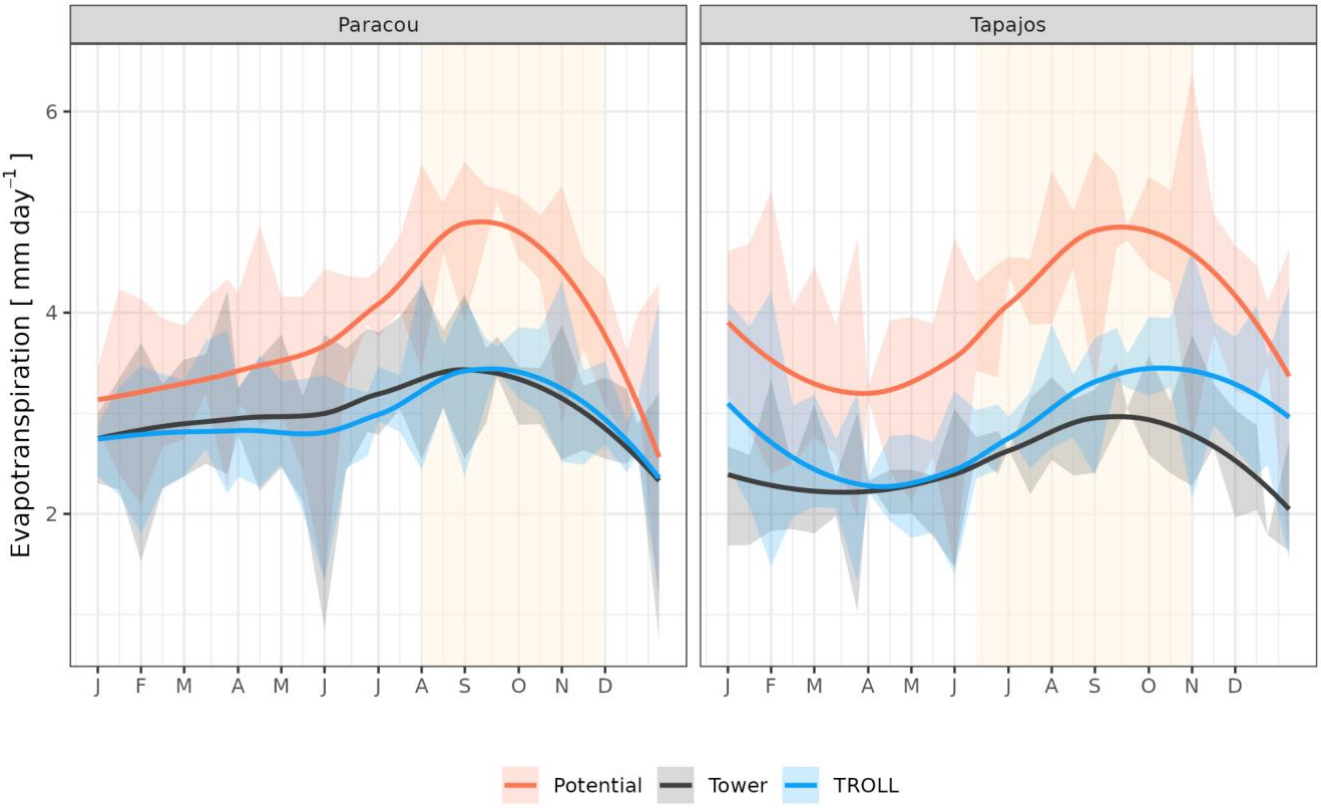

Figure 10: Mean annual cycle of evapotranspiration for Paracou and Tapajos, derived from fortnightly means. The red lines represent the potential evapotranspiration according to the Penman–Monteith equation, while the black lines represent the evapotranspiration derived from eddy-flux measurements and the blue lines the simulated evapotranspiration with TROLL 4.0. Bands are the intervals of means across years, and the yellow vertical bands in the background correspond to the site's climatological dry season. Simulated values correspond to 10 years of simulations starting from the end-state of 600-year regeneration from bare soil with calibrated parameters at each site. Inter-annual variations are shown in Figure S5.

Both eddy-flux-derived and simulated GPP showed a positive logarithmic relationship with cumulative incoming PAR and maximum VPD, as well as a positive linear relationship with mean temperature at daily scale (Fig. 11). However, TROLL 4.0 predicted a higher PAR conversion to carbon under high irradiance, VPD and temperature conditions in comparison to eddy-flux estimates, consistent with the higher dry-season GPP in simulations (Fig. 9). Responses of SIF-derived GPP to climatic variables were weak in comparison to simulated and eddy-flux derived GPP. Simulated ET was positively correlated with maximum VPD, cumulative PAR and mean temperature, similarly to eddy-flux derived ET (Fig. 12). At Paracou, the relationships between environmental drivers and simulated ET matched the ones obtained with eddy-flux estimates very closely, however simulated ET was overestimated under high irradiance, VPD, temperature and windy conditions in comparison to eddy-flux estimates at Tapajos.

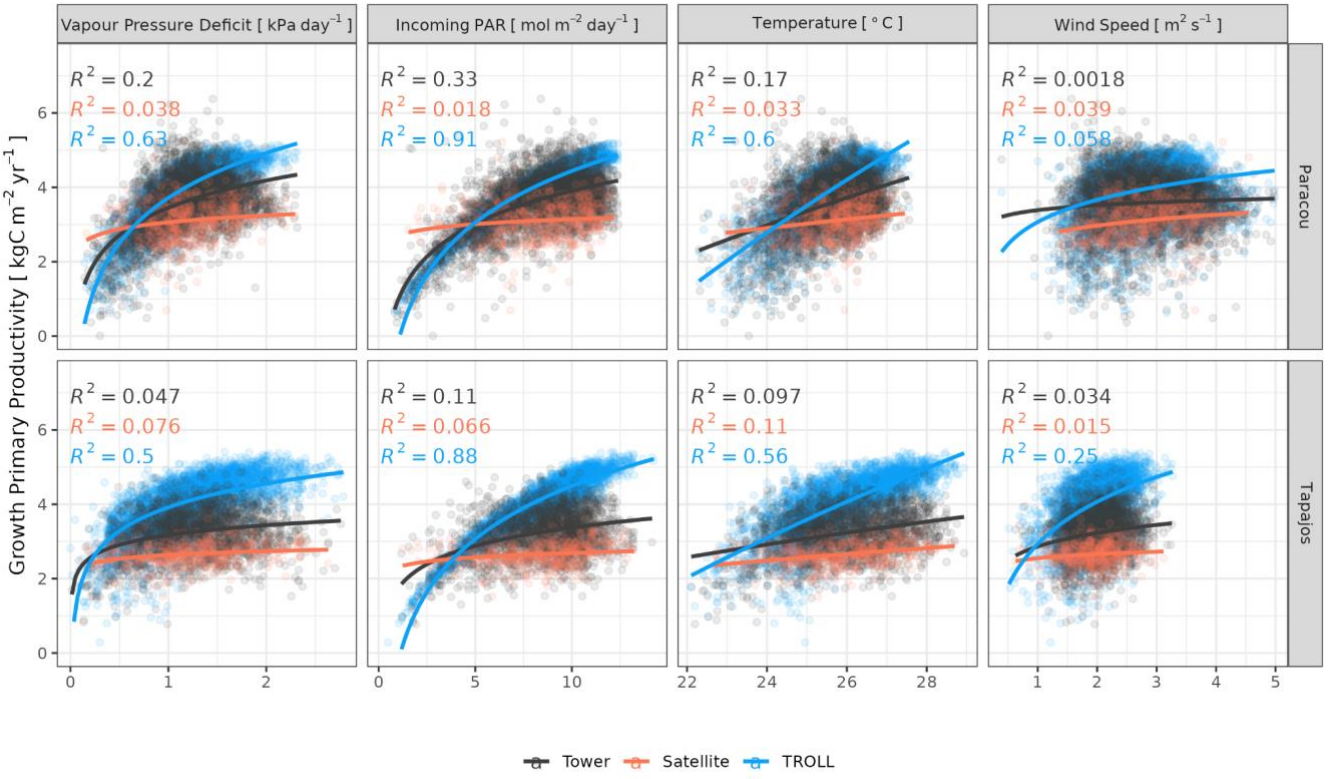

Figure 11: Daily averages of gross primary productivity as a function of daily maximum vapour pressure deficit, total incoming photosynthetically active radiation, average temperature, and average wind speed for model-, satellite- and eddy-flux-based estimates at Paracou (top) and Tapajos (bottom). Lines illustrate the linear regression of form y ~ log(x), and text the squared Pearson's R correlation coefficient.

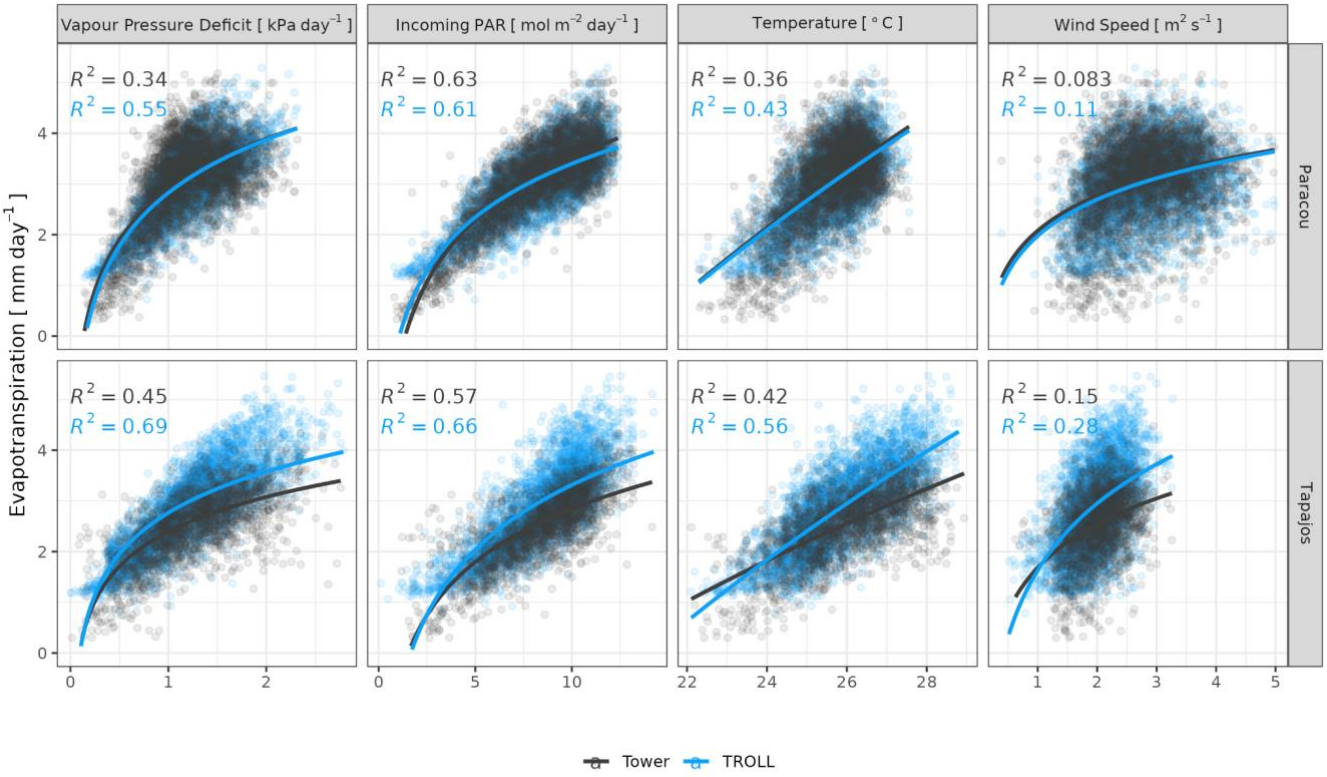

Figure 12: Daily total evapotranspiration as a function of daily maximum vapour pressure deficit, total incoming photosynthetically active radiation, average temperature, and average wind speed for model- and eddy-flux estimates at Paracou and Tapajos. Lines are illustrating the linear regression of form y ~ log(x), and text the squared Pearson's R correlation coefficient.

4 Discussion

Here we tested whether TROLL 4.0 was able to maintain the capacity of previous model's versions to reproduce observed forest structure and diversity, while simulating water and carbon fluxes between the forest ecosystem and the atmosphere, as well as leaf dynamics at fine temporal scales. We conducted a detailed model evaluation for two Amazonian rainforest sites, Paracou and Tapajos, presenting contrasting climate and soil properties. Both sites have been heavily monitored over the past decades. Yet it remains difficult to gather reliable data on a range of processes and spatial and temporal scales in order to make a solid assessment of the model. Here we compared the model outputs with the available data. We now discuss the consistencies and discrepancies between simulated and observed patterns, potential uncertainties in our results, and the advantages and limitations of TROLL 4.0 to simulate ecosystem properties such as forest structure and forest diversity, water and carbon fluxes, or leaf area.

4.1 Forest structure and composition

As for the previous versions, TROLL 4.0 jointly simulated realistic forest structure and species composition (Maréchaux et Chave, 2017). While the calibration of three global parameters led to simulated tree abundances across size classes and basal area or aboveground biomass in very good agreement with observations from forest inventories, aerial and satellite lidar data allowed forest structure to be assessed independently of calibration data. This revealed a very good ability of TROLL 4.0 to simulate the horizontal and vertical structure of the forest, which is promising for various applications, including biomass estimates (Knapp et al., 2018). Noteworthy, although coarser, the satellite data can prove useful for evaluating TROLL 4.0 and could be leveraged for model calibration with a global and freely available product in lack of finer-scale aerial- or drone-based scanning (Fischer et al., 2019). Understory inventories at Paracou also allowed us to independently evaluate TROLL 4.0's ability to simulate tree community structure in the 1-10-cm tree diameter range. TROLL 4.0 simulated the distribution of smaller trees reasonably well, although underrepresenting individuals from the smallest cohort. This underestimated density of small trees can partly be explained by the fact that the metric resolution of the aboveground voxel grid used in TROLL 4.0 allows only one tree per square metre ground while smaller trees can be tightly packed in some understory places. Explorations of simulated micro-environmental variations within the canopy (de Frenne et al., 2019) and inclusion of trait ontogenetic shifts (Fortunel et al., 2019) could further help understand and improve TROLL's ability to simulate forest structure in the understory.

TROLL 4.0 attributes individual trees to botanical species while allowing tree functional traits to vary within species. It thus provides a finer-grained description of biodiversity compared to models based on plant functional types (e.g. Longo et al., 2018), and uses a description matching the one of ecologists, in contrast with taxonomy-free continuous trait spectrum approaches (e.g. Sakschewski et al., 2015). The simulated species composition presented classically observed L-shaped profile of species rank abundance distribution in the two sites, but with an over-estimated species evenness resulting in under abundant dominant species and over abundant rare species, as already observed in previous versions of the model (Maréchaux and Chave, 2017). Several simulation factors could have resulted in the overestimation of species evenness, including functional trait species-specific values and the composition and strength of the external seed rain. Species trait values have been extracted from global databases that may not represent the actual average regional values for the Central Amazon or Guiana Shield regions, which might affect individual species behaviour in the model, but should not specifically affect evenness however. Moreover, trait values imputation for missing tree allometric parameters and turgor loss point with predictive mean matching may have disadvantaged dominant species or oppositely advantaged rare species, but it seems unlikely that the few imputations explained the whole evenness overestimation. Lastly, and more likely, the simulations used an external seed rain representing immigration in the simulated forest from a continuous forest matrix. The external seed rain maintains diversity in the simulated forest with a rescue effect, and if strong enough it can also prevent the hyper abundance of dominant species by minimising the recruitment limitation of less dominant species through a high immigration. As explained earlier, the composition of this external seed rain is assumed homogeneous across species, so that the simulated composition after regeneration from bare

ground is determined by species traits and their simulated effect on demographic processes and species fitness, rather than prescribed differences in seed rain. The effects of the representation of seed production, dispersal and recruitment on simulated communities should be further explored in the future, especially for projections under disturbance scenarios where forest regeneration is key (Diaz-Yanez et al., 2024, Hanbury-Brown et al., 2022).

TROLL 4.0 also explicitly simulates forest functional diversity characterised with functional trait distributions in the community. Simulated distributions matched well the observed distributions at both sites, as already observed in previous versions of the model (Maréchaux and Chave, 2017). In Paracou, the main discrepancies were the lack of individuals with high LMA (between 120 and 150 $g.m^{-2}$), low wood specific gravity (below 0.4 $g.cm^{-3}$) and/or high leaf area (above 100 cm^2). In contrast, in Tapajos, the model tended to simulate lower LMA and less negative turgor loss points on average. Since trait combinations are structured at the species level, and trait integration is high dimensional in tropical forests, with decoupled leaf and wood economic spectra (Baraloto et al., 2010) and weak associations between leaf turgor loss point and other leaf traits (Maréchaux et al., 2019), these discrepancies can be more easily interpreted at Paracou where the trait distributions are built on species-level (and not genus-level) information. Regarding the lack of high LMA individuals, TROLL 4.0 underestimated the abundance of common high LMA species such as *Lecythis persistence* or *Licania alba*. These species come from genera that are hyperdominant across the Amazon basin (ter Steege et al., 2013) but may be underrepresented in the simulations due to the overestimation of species evenness in TROLL 4.0 as discussed above. The lack of light wood and high leaf area individuals can be related to the underestimated abundances of pioneer species with fast growth (Chave et al., 2009) of the genera *Cecropia*, *Sterculia* and *Perebea*. These species are known to quickly colonise forest gaps under high light conditions, thanks to fast carbon assimilation and growth, and the dispersal of a high number of small, potentially dormant, seeds, leading to an omnipresence of these species in the forest seed bank (Holthuijzen and Boerboom, 1982; Alvarez-Buylla and Martínez-Ramos, 1990). In TROLL 4.0, the seed-size mediated tolerance-fecundity trade-off (Muller-Landau et al., 2010) is assumed to be perfectly equalising, and all species present in the local seed bank and able to strive under the local light availability have the same probability to be recruited. Such assumption is very likely detrimental to the recruitment of gap-affiliated species with a colonisation strategy, and this could be easily revisited in the future.

4.2 Leaf phenology

We calibrated and evaluated the new phenology module of TROLL 4.0. The calibration of the three module parameters ($a_{T,o}$, $b_{T,o}$ and δ_o), which together control the variation of old leaf fall under drying conditions, was conducted using litterfall trap data. This resulted in a realistic litterfall seasonality with a peak during the dry season as documented elsewhere (Manoli et al., 2018, Chave et al., 2010, van Langenhove et al., 2020). Interestingly, the calibration resulted in the same values for two parameters at the two sites ($a_{T,o}$, $b_{T,o}$) and close values for the third one (δ_o) to which the simulated litterfall pattern is less sensitive (Fig. S2). Simulations with the mean value of the third parameter at both sites resulted in similar evaluations (not

shown). This suggests a good transferability of the phenology module across sites without the need of site-specific calibration, although this remains to be further tested at additional sites and in contrasted conditions (e.g. Restrepo-Coupe et al., 2017). Acceleration of old leaf shedding was assumed to depend on soil water potential in the root zone, rather than soil water content, on individual leaf water potential at turgor loss point, and on tree size. These are biologically reasonable hypotheses and are in favour of a good generality of the module. We did notice that the current implementation of leaf dynamics in TROLL 4.0 leads to an underestimation of the basal flux of litterfall across months, in particular during the wet season, and, as a result, of total annual litterfall at both sites. In TROLL 4.0, leaf lifespan was parameterized based on empirical relationships with leaf structure (leaf mass per area), and the reliability and transferability of these empirical relationships would deserve more in-depth exploration. Alternative representations, such as the ones based on optimality principles (Kikuzawa 1991, Franklin et al., 2020, Manzoni et al., 2015), and their combination with the environmentally-driven old leaf shedding acceleration implemented in the new module could be explored in the future.

The evaluation of leaf area index (LAI) and its dynamics was difficult due to the number of products that yield inconsistent time series. Remotely sensed MODIS LAI showed a very small seasonal variation with a slight increase of LAI starting at the beginning of the dry season at both sites. However, MODIS LAI data products are known to be susceptible to the uncertainty affecting the bidirectional reflectance, and to saturate at high LAI values among others (Petri and Galvão, 2019). Local measurements of LAI through UAV-borne lidar in Paracou showed a stronger increase of total LAI of 0.5 $m^2.m^{-2}$ starting at the beginning of the dry season, and leading to a maximum in the dry season. This pattern of variation was in strong agreement with that simulated for LAI by TROLL 4.0. Similarly, local measurements of top canopy LAI derived from phenological cameras in Tapajos (Wu et al., 2016) also showed a high increase of total LAI in the dry season, above 0.5 $m^2.m^{-2}$, also in good agreement with the seasonal LAI variation simulated by TROLL 4.0 at that site. By contrast, the LAI derived from terrestrial vertical lidar in Tapajos showed almost no variations (Smith et al., 2019), and such differences with both the patterns derived from phenological cameras and simulations need to be further scrutinised. Among potential explanations, LAI from TLS in Tapajos was adjusted to the annual mean of 5.7 (Stark et al., 2012), leading to lower absolute variations than what was obtained elsewhere and used coarse spatial and temporal resolutions over small spatial and temporal extents (see material and methods). The discrepancy with simulated patterns could also be linked to uncertainties in LAI variations in the understory in our simulations. Recent studies have suggested opposite variations in LAI between the canopy and the understorey (Nunes et al., 2022), which should be further explored with TROLL 4.0. Overall, while obtaining robust estimate of LAI temporal variations in tropical forests remain a huge challenge (Vincent et al., 2023; Bai et al., 2023), the relative variation of LAI simulated by TROLL 4.0 was in very good agreement with one of the most reliable products at each site, providing a first encouraging assessment of this model's ability. Importantly, while total LAI variation remains limited on average within a year in tropical rainforests, this hides important turnover across leaf ages and species, and for the sake of prediction robustness, models should endeavour to represent such turnover and its underlying processes (Wu et al., 2017).

The dry-season increase in total LAI simulated in TROLL 4.0 corresponds to a rejuvenation of the canopy associated with a decrease in the LAI of old leaves at the beginning of the dry season, directly followed by an increase in the LAI of young leaves during the dry season. This turnover is in very good agreement with the one captured by phenological cameras at Tapajos (Wu et al., 2016) and documented elsewhere (Yang et al., 2021; Doughty and Goulden, 2008), questioning the opposite young LAI pattern obtained from Yang et al. (2023)'s global reanalysis at this site. The main difference in simulated cohorts between the two sites is the continuous dominance of old LAI in Tapajos while mature leaves dominated at the end of the dry season in Paracou. This dominance of older (and less efficient) leaves in Tapajos may be linked to the underestimated litterfall flux and soil water depletion during the dry season at this site. However, the relative proportion of leaf area across the different leaf age pools within and across datasets strongly depends on the definition of the leaf age pools themselves. These pools depend on the individual leaf lifespan in TROLL 4.0 (see section 2.6.2 in Maréchaux et al., submitted companion paper), while the transition from young to mature and mature to old are respectively fixed to 1.71 and 5.14 months in Yang et al. (2023) and fitted to 1 and 3 months in Wu et al. (2016). These contrasting approaches may explain the higher relative importance of old leaves in Wu et al. (2016) compared to Yang et al. (2023) and the intermediate values of TROLL 4.0 (Fig. 6). The seasonal dynamics of leaf cohorts remains poorly known in tropical forests and additional high-resolution optical imagery, *e.g.* by drones or phenological cameras, would be extremely useful to better document these patterns.

4.3 Water and carbon fluxes

At Tapajos, DGVMs simulate seasonal trends in carbon and water fluxes opposite to the observed ones (e.g. Fig. 1 in Chen et al., 2020; Fig. 5 in Longo et al., 2019b; Fig. 3 in Restrepo-Coupe et al., 2017). In contrast, TROLL 4.0 showed a very good ability to represent the dynamics of both carbon and water fluxes estimated with eddy covariance data. In particular, TROLL 4.0 captures the dry season increase in gross primary productivity (GPP) and evapotranspiration (ET) documented for light-limited forests (Guan et al. 2017, Wagner et al. 2016, Aguilos et al. 2018). Simulated GPP and ET also presented realistic daily responses to environmental drivers, namely vapour pressure deficit (VPD), temperature, incident radiation and wind speed, both in direction and relative magnitude.

However, at Tapajos, we found that TROLL 4.0 overestimated ET during the dry season in comparison to eddy-flux-derived ET values, under high irradiance, VPD and temperature. Simulated ET consists in tree transpiration summed over simulated individuals, water evaporation from the topsoil layer, and the direct evaporation of the rainfall intercepted by the canopy (Kunert et al., 2017). As ET was faithfully simulated in Paracou and never exceeded the potential ET at Tapajos, TROLL 4.0 may underestimate the stomatal control of transpiration during the dry season at Tapajos. Accordingly, the control of ET by atmospheric conditions in Tapajos was overestimated in simulated data in comparison to observations, suggesting a stronger coupling of vegetation and atmosphere at that site than simulated (de Kauwe et al., 2017). Underestimation of stomatal control can result from the representation of stomatal conductance and its responses to soil water availability. These are active areas of research and alternative representations could be considered in the future (Wolf et al. 2016; Anderegg et al. 2018; Sabot et

al., 2022, Lamour et al., 2022; see sections 2.5.2 and 2.5.3 and Appendix B in Maréchaux et al. submitted companion paper). Alternatively, during the dry season, a lack of stomatal control can be due to an overestimation of soil water availability in the model. Soil water content dynamics depend on both the soil depth (Fig. S7) and on the soil hydraulic properties. The two sites are known to present heterogeneity in soil properties but we here performed simulations with homogenous soil properties, both horizontally and vertically. For instance in Paracou, the topsoil layer is sandier than the 15-30 cm layer (Van Langenhove et al., 2021). Although TROLL 4.0 quantitatively captures the soil water depletion observed during the dry season, it appears to underestimate this depletion compared to isolated measurements at Paracou (Fig. S6). This underestimation occurs despite the simulated total ET being in quantitative agreement with eddy covariance data during the dry season in Paracou. Testing the model's sensitivity to soil layer thickness and properties will be important to perform prior to forest projections under drier future conditions and model spatial up-scaling (Meunier et al., 2022). For example, simulations with the ED2 model suggested that forest responses to drier conditions at Tapajos strongly depended on soil texture (Longo et al., 2018).

TROLL 4.0 tended to overestimate GPP, particularly during the dry season, in comparison to both eddy-covariance- and SIF-derived GPP. GPP is driven by the photosynthetic activity of the canopy, which depends on multiple processes and further work would be needed to precisely discriminate among them, while accounting for eddy-covariance uncertainties (Cui and Chui, 2019). Among others, simulated GPP is sensitive to the parameters that control light diffusion and uptake (light extinction coefficient, apparent quantum yield; Maréchaux & Chave, 2017). Both are assumed fixed and constant in simulations, but are known to vary with leaf angle and thickness, depending on micro-environmental conditions and species (Long et al., 1993; Poorter et al., 1995; Meir et al., 2000; Kitajima et al., 2005). Similarly, the response of leaf-level gas exchanges to soil water availability shows no clear consensus across models (Powell et al, 2013; Trugman et al., 2018), and could be underestimated during the dry season in TROLL 4.0 simulations. Simulated GPP was higher than inferred from eddy-covariance data, which was itself higher than GPP inferred from SIF satellite data (Chen et al., 2022). Even though solar induced fluorescence offers a great potential for the evaluation or the calibration of seasonal carbon fluxes in vegetation models, especially as the tropics are underrepresented by eddy-flux tower networks (Villarreal et Vargas, 2021), current SIF products should be used with great care.

5 Conclusions

Here we evaluated the TROLL 4.0 individual-based forest dynamics model, which is capable of jointly simulating the structure, diversity and functioning. To this end, we assembled data from forest inventories, eddy-flux towers, litterfall traps, UAV-borne and terrestrial lidar, phenological cameras, and satellite products at two Amazonian forest sites and found that TROLL 4.0 was able to realistically simulate the forest structure and composition, water and carbon fluxes, and leaf area dynamics. In using data of different nature and under the control of different processes, we limited the emergence of equi-finality issues (Medlyn et al., 2005), suggesting a good transferability and robustness of TROLL 4.0.

Comparison with field inventories, aerial and satellite data confirm TROLL 4.0's ability to realistically simulate the structure and composition of tropical forests, without imposing constraints beyond the species pool. Discrepancies between observed and simulated tree abundances in small size classes and abundance of trait values specific to colonising species suggest further developments of regeneration processes, a worthy endeavour in the context of increased disturbance regimes. TROLL 4.0 was further able to simultaneously simulate the seasonality of productivity, evapotranspiration and leaf area in these two light-limited forests, as opposed to many current DGVMs (Chen et al., 2020; Restrepo-Coupe et al., 2017; Longo et al., 2019). The model robustness to simulate ecosystem fluxes is further suggested by the responses of carbon and water fluxes to environmental drivers, whose direction and relative importance were well aligned with observations at both sites despite contrasting climate and soil properties. Additionally, the dynamics of total leaf area appeared realistically partitioned into different leaf pools, as shown by the leaf rejuvenation during the dry season in these systems (Wu et al., 2016; Yang et al., 2021). However, further inspection of the leaf area dynamics across the canopy vertical profile would be useful. Also, the model overestimation of productivity and evapotranspiration during the dry season calls for a more in-depth exploration of the model representation of respiration as well as stomatal control.

Overall, our analyses establish the suitability of TROLL 4.0 for simulating forest structure, diversity and ecosystem functioning in short- and long-term studies of tropical forest dynamics, paving the way for multiple applications (Maréchaux et al., 2021). TROLL 4.0 could thus be used for projections of the effects of climate change on tropical forests, and exploration of the effect of biodiversity on forest resilience to these changes (Sakschewski et al., 2016). Similarly, as TROLL 4.0 retains the species-level taxonomic description, it can also help explore the effects of management practices such as timber production, for which half of tropical forests are designated (Blaser et al., 2011). While the development of TROLL 4.0 will continue, in light of knowledge improvement, novel data collection and identification of uncertainties and discrepancies, we believe it represents a valuable tool for addressing the major challenges tropical forests are currently facing.

Code and data availability

The TROLL version 4.0 and further developments are publicly available on GitHub as a C++ standalone at https://github.com/TROLL-code/TROLL or wrapped into an R package at https://github.com/sylvainschmitt/rcontroll/. All the code associated with the analyses described in this paper are available at https://github.com/sylvainschmitt/troll_eval and permanently stored at add a zenodo doi after acceptance with corresponding analyses notebook at https://sylvainschmitt.github.io/troll_eval/. Inventories data for Paracou trees over 10 cm are available through request, PI: GD, on the CIRAD dataverse: https://dataverse.cirad.fr/dataverse/paracou. Paracou trees understory trees are available through request, PI: GS, GD, JC. Aerial Lidar Scanning from Paracou are available through request (PI: GV) and from dos-Santos et al. (2019) for Tapajos. Species data are available from Jucker et al., (2022), Maréchaux et al., (2015), Guillemot et al., (2022),

Vleminckx et al., (2021), Maréchaux et al., (2019), Nemetschek et al., (2024), Schmitt and Boisseaux (2023), Boisseaux et al., (submitted), Ziegler et al., (2019), Baraloto et al., (2010), and from TRY (Kattge, Bönisch, et al., 2020). Soil data have been collected from Van Langenhove et al., (2021), Silver et al., (2000), Quesada et al., (2010), Sabatier et al., (1997), and Nepstad et al., (2002). Eddy covariance data from Paracou and Tapajos sites are available on FLUXNET at https://fluxnet.fluxdata.org (last access: 6 September 2023). ERA5-Land data are available on the Climate Data Store: https://cds.climate.copernicus.eu/cdsapp#!/dataset/reanalysis-era5-land?tab=overview. TROPOMI SIF satellite data are available in Chen et al., (2022). Litterfall data at Tapajos are available online through the Oak Ridge National Laboratory (ORNL) Distributed Active Archive Center (DAAC): https://daac.ornl.gov/LBA/guides/CD10_Litter_Tapajos.html and upon-request at Paracou, PI: DB. MODIS LAI data are available online and were extracted from PLUMBER2 on Research Data Australia: https://researchdata.edu.au/plumber2-forcing-evaluation-surface-models/1656048. Terrestrial LAD data from Tapajos are available in Smith et al., (2019). Lidar PAD data from Paracou are available upon-request, PIs: NB and GV. LAI variations among young, mature and leaf cohorts are available from the reanalysis of Yang et al. (2023) at: https://figshare.com/articles/dataset/Leaf_age-dependent_LAI_seasonality_product_Lad-LAI_over_tropical_and_subtropical_evergreen_broadleaved_forests/21700955/4 and from the phenological camera of Wu et al., (2016) at: https://datadryad.org/stash/dataset/doi:10.5061/dryad.8fb47.

Supplement

The supplement related to this article is available below.

Author contributions

SS and IM designed the model assessment and carried out the TROLL 4.0 simulations. SS, FJF, JC and IM developed TROLL 4.0. SS, FJF, NB, MB, DB, BB, XC, GD, JL, DM, NRC, ScS, GS, PV, GV, CZ, JC, IM contributed to the data collection and compilation. SS and IM wrote the paper.

Competing interests

The authors declare that they have no conflict of interest.

Acknowledgements

We are particularly grateful to all the ground workers and data collectors (forest inventories, eddy flux measurements, litter traps, lidar acquisition, sampling and measurement of functional traits, and more) who are not named here but who contributed to the vast knowledge base without which the evaluation of TROLL 4.0 would have been impossible. We are grateful to the

GenoToul bioinformatics facility (Castanet-Tolosan, Toulouse, Occitanie, France, doi:10.15454/1.5572369328961167E12) for providing computing resources.

Financial support

This research has been supported by fundings from ANR (the French National Research Agency) under the "Investissements d'avenir" program with the references ANR-16-IDEX-0006, ANR-10-LABX-25-01, ANR-10-LABX-0041, the Amazonian Landscapes in Transition ANR project (ALT), CNES Biomass-Valo project, and ESA CCI-BIOMASS.

References

Aguilos, M., Hérault, B., Burban, B., Wagner, F., and Bonal, D.: What drives long-term variations in carbon flux and balance in a tropical rainforest in French Guiana?, Agricultural and Forest Meteorology, 253–254, 114–123, https://doi.org/10.1016/j.agrformet.2018.02.009, 2018.

Alvarez-Buylla, E. R., & Martinez-Ramos, M. (1992). Demography and allometry of Cecropia obtusifolia, a neotropical pioneer tree-an evaluation of the climax-pioneer paradigm for tropical rain forests. *Journal of Ecology*, 275-290.

Aragão, L. E. O. C., Malhi, Y., Metcalfe, D. B., Silva-Espejo, J. E., Jiménez, E., Navarrete, D., ... & Vásquez, R. (2009). Above-and below-ground net primary productivity across ten Amazonian forests on contrasting soils. *Biogeosciences*, *6*(12), 2759-2778.

Baraloto, C., Paine, R., Patiño, S., Bonal, D., Hérault B., and Chave, J.: Functional Trait Variation and Sampling Strategies in Species-Rich Plant Communities, Functional Ecology, 24, 208–16. https://doi.org/10.1111/j.1365-2435.2009.01600.x, 2010.

Bai, Y., Durand, J. B., Vincent, G., & Forbes, F. (2024). Semantic segmentation of sparse irregular point clouds for leaf/wood discrimination. *Advances in Neural Information Processing Systems*, *36*.

Baraloto, C., Timothy Paine, C. E., Poorter, L., Beauchene, J., Bonal, D., Domenach, A. M., ... & Chave, J. (2010). Decoupled leaf and stem economics in rain forest trees. *Ecology letters*, *13*(11), 1338-1347.

Berzaghi, F., Wright, I. J., Kramer, K., Oddou-Muratorio, S., Bohn, F. J., Reyer, C. P. O., Sabaté, S., Sanders, T. G. M., and Hartig, F.: Towards a New Generation of Trait-Flexible Vegetation Models, Trends in Ecology & Evolution, 35, 191–205, https://doi.org/10.1016/j.tree.2019.11.006, 2020.

Boisseaux et al. submitted

BONAL, DAMIEN, ALEXANDRE BOSC, STÉPHANE PONTON, JEAN-YVES GORET, BENOÎT BURBAN, PATRICK GROSS, JEAN-MARC BONNEFOND, et al. 2008. "Impact of Severe Dry Season on Net Ecosystem Exchange in the Neotropical Rainforest of French Guiana." Global Change Biology 14 (8): 1917–33. https://doi.org/10.1111/j.1365-2486.2008.01610.x.

Bonan, G. B.: Forests and Climate Change: Forcings, Feedbacks, and the Climate Benefits of Forests, Science, 320, 1444–1449. https://doi.org/10.1126/science.1155121, 2008

Bugmann, H.: A review of forest gap models, Climatic Change, 51, 259–305, https://doi.org/10.1023/A:1012525626267, 2001.

Chave, J., Andalo, C., Brown, S., Cairns, M.A., Chambers, J.Q., Eamus, D., Fölster, H., Fromard, F., Higuchi, N., Kira, T., Lescure, J.P., Nelson, B.W., Ogawa, H., Puig, H., Riéra, B. & Yamakura, T. (2005). Tree allometry and improved estimation of carbon stocks and balance in tropical forests. Oecologia, 145, 87–99.

Chave, J., Navarrete, D., Almeida, S., Álvarez, E., Aragão, L. E., Bonal, D., ... & Malhi, Y. (2010). Regional and seasonal patterns of litterfall in tropical South America. *Biogeosciences*, *7*(1), 43-55.

Chen, X., Maignan, F., Viovy, N., Bastos, A., Goll, D., Wu, J., ... & Ciais, P. (2020). Novel representation of leaf phenology improves simulation of Amazonian evergreen forest photosynthesis in a land surface model. *Journal of Advances in Modeling Earth Systems*, *12*(1), e2018MS001565.

Chen, Xingan, Yuefei Huang, Chong Nie, Shuo Zhang, Guangqian Wang, Shiliu Chen, and Zhichao Chen. 2022. "A Long-Term Reconstructed TROPOMI Solar-Induced Fluorescence Dataset Using Machine Learning Algorithms." Scientific Data 9 (1). https://doi.org/10.1038/s41597-022-01520-1.

Cuartas, L. A., Tomasella, J., Nobre, A. D., Hodnett, M. G., & Múnera, J. C. (2007). Interception water-partitioning dynamics for a pristine rainforest in Central Amazonia: marked differences between normal and dry years. *Agricultural and Forest Meteorology*, *145*(1-2), 69-83.

Cui, W., & Chui, T. F. M. (2019). Temporal and spatial variations of energy balance closure across FLUXNET research sites. *Agricultural and forest meteorology*, *271*, 12-21.

Cusack, D. F., Christoffersen, B., Smith-Martin, C. M., Andersen, K. M., Cordeiro, A. L., Fleischer, K., ... & Norby, R. J. (2024). Toward a coordinated understanding of hydro-biogeochemical root functions in tropical forests for application in vegetation models. *New Phytologist*.

De Frenne, P., Zellweger, F., Rodríguez-Sánchez, F., Scheffers, B. R., Hylander, K., Luoto, M., ... & Lenoir, J. (2019). Global buffering of temperatures under forest canopies. *Nature Ecology & Evolution*, *3*(5), 744-749.

De Kauwe, M. G., Medlyn, B. E., Knauer, J., & Williams, C. A. (2017). Ideas and perspectives: how coupled is the vegetation to the boundary layer?. *Biogeosciences*, *14*(19), 4435-4453.

Derroire, G., Hérault, B., Rossi, V., Blanc, L., Gourlet- Fleury, S., & Schmitt, L. (2023). Paracou permanent plots. CIRAD Dataverse. https://doi.org/10.18167/DVN1/8G8AHY

Díaz-Yáñez, O., Käber, Y., Anders, T., Bohn, F., Braziunas, K. H., Brůna, J., ... & Bugmann, H. (2024). Tree regeneration in models of forest dynamics: A key priority for further research. *Ecosphere*, *15*(3), e4807.

Dormann, C. F., Schymanski, S. J., Cabral, J., Chuine, I., Graham, C., Hartig, F., Kearney, M., Morin, X., Römermann, C., Schröder, B., and Singer, A.: Correlation and process in species distribution models: bridging a dichotomy, Journal of Biogeography, 39, 2119–2131, https://doi.org/10.1111/j.1365-2699.2011.02659.x, 2012.

dos-Santos, M.N., M.M. Keller, and D.C. Morton. 2019. LiDAR Surveys over Selected Forest Research Sites, Brazilian Amazon, 2008-2018. ORNL DAAC, Oak Ridge, Tennessee, USA. https://doi.org/10.3334/ORNLDAAC/1644; https://www.paisagenslidar.cnptia.embrapa.br/geonetwork/

Doughty, C. E., & Goulden, M. L. (2008). Seasonal patterns of tropical forest leaf area index and CO2 exchange. *Journal of Geophysical Research: Biogeosciences*, *113*(G1).

Duursma, R. A., Blackman, C. J., Lopéz, R., Martin-StPaul, N. K., Cochard, H., & Medlyn, B. E. (2019). On the minimum leaf conductance: its role in models of plant water use, and ecological and environmental controls. *New Phytologist*, *221*(2), 693-705.

Eegholm, B., Wake, S., Denny, Z., Dogoda, P., Poulios, D., Coyle, B., ... & Blair, B. (2019, August). Global Ecosystem Dynamics Investigation (GEDI) instrument alignment and test. In Optical Modeling and System Alignment (Vol. 11103, pp. 53-70). SPIE.

Estes, L., Elsen, P. R., Treuer, T., Ahmed, L., Caylor, K., Chang, J., ... & Ellis, E. C. (2018). The spatial and temporal domains of modern ecology. *Nature ecology & evolution*, *2*(5), 819-826.

Evans, M. R.: Modelling ecological systems in a changing world, Phil. Trans. R. Soc. B, 367, 181–190, https://doi.org/10.1098/rstb.2011.0172, 2012.

Farquhar, G. D., von Caemmerer, S. V., & Berry, J. A. (1980). A biochemical model of photosynthetic CO 2 assimilation in leaves of C 3 species. planta, 149, 78-90.

Fischer, F. J., Maréchaux, I., & Chave, J. (2019). Improving plant allometry by fusing forest models and remote sensing. *New Phytologist*, *223*(3), 1159-1165.

Fisher, J. B., Huntzinger, D. N., Schwalm, C. R., and Sitch, S.: Modeling the Terrestrial Biosphere, Annual Review of Environment and Resources, 39, 91–123, https://doi.org/10.1146/annurev-environ-012913-093456, 2014.

Fisher, R. A., Muszala, S., Verteinstein, M., Lawrence, P., Xu, C., McDowell, N. G., Knox, R. G., Koven, C., Holm, J., Rogers, B. M., Spessa, A., Lawrence, D., and Bonan, G.: Taking off the training wheels: the properties of a dynamic vegetation model without climate envelopes, CLM4.5(ED), Geosci. Model Dev., 8, 3593–3619, https://doi.org/10.5194/gmd-8-3593-2015, 2015.

Fischer, R., Bohn, F., de Paula, M. D., Dislich, C., Groeneveld, J., Gutiérrez, A. G., ... & Huth, A. (2016). Lessons learned from applying a forest gap model to understand ecosystem and carbon dynamics of complex tropical forests. *Ecological modelling*, *326*, 124-133.

Fischer, F. J., Jackson, T. D., Vincent, G., & Jucker, T. (2024). Robust characterization of forest structure from airborne laser scanning-a systematic assessment and sample workflow for ecologists. *bioRxiv*, 2024-03.

Fisher, R. A., Koven, C. D., Anderegg, W. R. L., Christoffersen, B. O., Dietze, M. C., Farrior, C. E., Holm, J. A., Hurtt, G. C., Knox, R. G., Lawrence, P. J., Lichstein, J. W., Longo, M., Matheny, A. M., Medvigy, D., Muller-Landau, H. C., Powell, T. L., Serbin, S. P., Sato, H., Shuman, J. K., Smith, B., Trugman, A. T., Viskari, T., Verbeeck, H., Weng, E., Xu, C., Xu,

X., Zhang, T., and Moorcroft, P. R.: Vegetation demographics in Earth System Models: A review of progress and priorities, Global Change Biology, 24, 35–54, https://doi.org/10.1111/gcb.13910, 2018.

Fortunel, C., Stahl, C., Heuret, P., Nicolini, E., & Baraloto, C. (2020). Disentangling the effects of environment and ontogeny on tree functional dimensions for congeneric species in tropical forests. *New Phytologist*, *226*(2), 385-395.

Franklin, O., Harrison, S. P., Dewar, R., Farrior, C. E., Brännström, Å., Dieckmann, U., ... & Prentice, I. C. (2020). Organizing principles for vegetation dynamics. *Nature plants*, *6*(5), 444-453.

Fu, Rong, Lei Yin, Wenhong Li, Paola A. Arias, Robert E. Dickinson, Lei Huang, Sudip Chakraborty, et al. 2013. "Increased Dry-Season Length over Southern Amazonia in Recent Decades and Its Implication for Future Climate Projection." Proceedings of the National Academy of Sciences 110 (45): 18110–15. https://doi.org/10.1073/pnas.1302584110.

Goncalves, F.G., R.N. Treuhaft, J.R. Dos santos, P. Graca, A. Almeida, and B.E. Law. 2018. Tree Inventory and Biometry Measurements, Tapajos National Forest, Para, Brazil, 2010. ORNL DAAC, Oak Ridge, Tennessee, USA. https://doi.org/10.3334/ORNLDAAC/1552

Gourlet-Fleury, S., Guehl, J. M. J. M., & Laroussinie, O. (2004). *Ecology and management of a neotropical rainforest. Lessons drawn from Paracou, a long-term experimental research site in French Guiana* (pp. 350-p). Elsevier.

Guan, K., Pan, M., Li, H., Wolf, A., Wu, J., Medvigy, D., Caylor, K. K., Sheffield, J., Wood, E. F., Malhi, Y., Liang, M., Kimball, J. S., Saleska, S. R., Berry, J., Joiner, J., and Lyapustin, A. I.: Photosynthetic seasonality of global tropical forests constrained by hydroclimate, Nature Geosci, 8, 284–289, https://doi.org/10.1038/ngeo2382, 2015.

Guillemot, Joannès, Nicolas K. Martin-StPaul, Leticia Bulascoschi, Lourens Poorter, Xavier Morin, Bruno X. Pinho, Guerric le Maire, et al. 2022. "Small and Slow Is Safe: On the Drought Tolerance of Tropical Tree Species." Global Change Biology 28 (8): 2622–38. https://doi.org/10.1111/gcb.16082.

Hanbury-Brown, A. R., Ward, R. E., & Kueppers, L. M. (2022). Forest regeneration within Earth system models: current process representations and ways forward. *New Phytologist*, *235*(1), 20-40.

Harper, A., Baker, I. T., Denning, A. S., Randall, D. A., Dazlich, D., and Branson, M.: Impact of evapotranspiration on dry season climate in the Amazon forest, Journal of Climate, 27, 574–591, https://doi.org/10.1175/JCLI-D-13-00074.1, 2013.

Holthuijzen, A. M. A., & Boerboom, J. H. A. (1982). The Cecropia seedbank in the Surinam lowland rain forest. *Biotropica*, 62-68.

Hubau, W., Lewis, S. L., Phillips, O. L., Affum-Baffoe, K., Beeckman, H., Cuní-Sanchez, A., Daniels, A. K., Ewango, C. E. N., Fauset, S., Mukinzi, J. M., Sheil, D., Sonké, B., Sullivan, M. J. P., Sunderland, T. C. H., Taedoumg, H., Thomas, S. C., White, L. J. T., Abernethy, K. A., Adu-Bredu, S., Amani, C. A., Baker, T. R., Banin, L. F., Baya, F., Begne, S. K., Bennett, A. C., Benedet, F., Bitariho, R., Bocko, Y. E., Boeckx, P., Boundja, P., Brienen, R. J. W., Brncic, T., Chezeaux, E., Chuyong, G. B., Clark, C. J., Collins, M., Comiskey, J. A., Coomes, D. A., Dargie, G. C., de Haulleville, T., Kamdem, M. N. D., Doucet, J.-L., Esquivel-Muelbert, A., Feldpausch, T. R., Fofanah, A., Foli, E. G., Gilpin, M., Gloor, E., Gonmadje, C., Gourlet-Fleury, S., Hall, J. S., Hamilton, A. C., Harris, D. J., Hart, T. B., Hockemba, M. B. N., Hladik, A.,

Ifo, S. A., Jeffery, K. J., Jucker, T., Yakusu, E. K., Kearsley, E., Kenfack, D., Koch, A., Leal, M. E., Levesley, A., Lindsell, J. A., Lisingo, J., Lopez-Gonzalez, G., Lovett, J. C., Makana, J.-R., Malhi, Y., Marshall, A. R., Martin, J., Martin, E. H., Mbayu, F. M., Medjibe, V. P., Mihindou, V., Mitchard, E. T. A., Moore, S., Munishi, P. K. T., Bengone, N. N., Ojo, L., Ondo, F. E., Peh, K. S.-H., Pickavance, G. C., Poulsen, A. D., Poulsen, J. R., Qie, L., Reitsma, J., Rovero, F., Swaine, M. D., Talbot, J., Taplin, J., Taylor, D. M., Thomas, D. W., Toirambe, B., Mukendi, J. T., Tuagben, D., Umunay, P. M., et al.: Asynchronous carbon sink saturation in African and Amazonian tropical forests, Nature, 579, 80–87, https://doi.org/10.1038/s41586-020-2035-0, 2020.

Huntingford, C., Atkin, O. K., Martinez-De La Torre, A., Mercado, L. M., Heskel, M. A., Harper, A. B., ... & Malhi, Y. (2017). Implications of improved representations of plant respiration in a changing climate. *Nature Communications*, *8*(1), 1602.

Joetzjer, E., Maignan, F., Chave, J., Goll, D., Poulter, B., Barichivich, J., Maréchaux, I., Luyssaert, S., Guimberteau, M., Naudts, K., Bonal, D., and Ciais, P.: Effect of tree demography and flexible root water uptake for modeling the carbon and water cycles of Amazonia, Ecological Modelling, 469, 109969, https://doi.org/10.1016/j.ecolmodel.2022.109969, 2022.

Jucker, Tommaso, Fabian Jörg Fischer, Jérôme Chave, David A. Coomes, John Caspersen, Arshad Ali, Grace Jopaul Loubota Panzou, et al. 2022. “Tallo: A Global Tree Allometry and Crown Architecture Database.” Global Change Biology 28 (17): 5254–68. https://doi.org/10.1111/gcb.16302.

Kattge, Jens, Gerhard Bönisch, and et al. 2020. “TRY Plant Trait Database – Enhanced Coverage and Open Access.” Global Change Biology 26: 119–88. https://doi.org/10.1111/gcb.14904.

Kikuzawa, K. (1991). A cost-benefit analysis of leaf habit and leaf longevity of trees and their geographical pattern. *The American Naturalist*, *138*(5), 1250-1263.

Koch, A., Hubau, W., and Lewis, S. L.: Earth System Models Are Not Capturing Present-Day Tropical Forest Carbon Dynamics, Earth’s Future, 9, e2020EF001874, https://doi.org/10.1029/2020EF001874, 2021.

Köster J, Rahmann S (2012) Snakemake-a scalable bioinformatics workflow engine. Bioinformatics, 28, 2520–2522. https://doi.org/10.1093/bioinformatics/bts480

Knapp, N., Fischer, R., & Huth, A. (2018). Linking lidar and forest modeling to assess biomass estimation across scales and disturbance states. *Remote Sensing of Environment*, *205*, 199-209.

Kunert, N., Aparecido, L. M. T., Wolff, S., Higuchi, N., dos Santos, J., de Araujo, A. C., & Trumbore, S. (2017). A revised hydrological model for the Central Amazon: The importance of emergent canopy trees in the forest water budget. *Agricultural and Forest Meteorology*, *239*, 47-57.

Kurtzer GM, Sochat V, Bauer MW (2017) Singularity: Scientific containers for mobility of compute. PLoS ONE, 12, 1–20. https://doi.org/10.1371/journal.pone.0177459

Lamour, J., Davidson, K. J., Ely, K. S., Le Moguédec, G., Leakey, A. D., Li, Q., ... & Rogers, A. (2022). An improved representation of the relationship between photosynthesis and stomatal conductance leads to more stable estimation of

conductance parameters and improves the goodness-of-fit across diverse data sets. *Global change biology*, *28*(11), 3537-3556.

Lapola, D. M., Pinho, P., Barlow, J., Aragão, L. E. O. C., Berenguer, E., Carmenta, R., Liddy, H. M., Seixas, H., Silva, C. V. J., Silva-Junior, C. H. L., Alencar, A. A. C., Anderson, L. O., Armenteras, D., Brovkin, V., Calders, K., Chambers, J., Chini, L., Costa, M. H., Faria, B. L., Fearnside, P. M., Ferreira, J., Gatti, L., Gutierrez-Velez, V. H., Han, Z., Hibbard, K., Koven, C., Lawrence, P., Pongratz, J., Portela, B. T. T., Rounsevell, M., Ruane, A. C., Schaldach, R., da Silva, S. S., von Randow, C., and Walker, W. S.: The drivers and impacts of Amazon forest degradation, Science, 379, eabp8622, https://doi.org/10.1126/science.abp8622, 2023.

Lawrence, D., & Vandecar, K. (2015). Effects of tropical deforestation on climate and agriculture. Nature climate change, 5(1), 27-36.

Long, S. P., Postl, W. F., & Bolhar-Nordenkampf, H. R. (1993). Quantum yields for uptake of carbon dioxide in C3 vascular plants of contrasting habitats and taxonomic groupings. *Planta*, *189*(2), 226-234.

Longo, M., Knox, R. G., Levine, N. M., Alves, L. F., Bonal, D., Camargo, P. B., ... & Moorcroft, P. R. (2018). Ecosystem heterogeneity and diversity mitigate Amazon forest resilience to frequent extreme droughts. *New Phytologist*, *219*(3), 914-931.

Longo, M., Knox, R. G., Medvigy, D. M., Levine, N. M., Dietze, M. C., Kim, Y., ... & Moorcroft, P. R. (2019). The biophysics, ecology, and biogeochemistry of functionally diverse, vertically and horizontally heterogeneous ecosystems: The Ecosystem Demography model, version 2.2–Part 1: Model description. *Geoscientific Model Development*, *12*(10), 4309-4346.

Longo, M., Knox, R. G., Medvigy, D. M., Levine, N. M., Dietze, M. C., Kim, Y., ... & Moorcroft, P. R. (2019). The biophysics, ecology, and biogeochemistry of functionally diverse, vertically and horizontally heterogeneous ecosystems: The Ecosystem Demography model, version 2.2–Part 2: Model evaluation for tropical South America.*Geoscientific Model Development*, *12*(10), 4309-4346.

Malhi, Y., Doughty, C., & Galbraith, D. (2011). The allocation of ecosystem net primary productivity in tropical forests. *Philosophical Transactions of the Royal Society B: Biological Sciences*, *366*(1582), 3225-3245.

Manzoni, S., Vico, G., Thompson, S., Beyer, F., & Weih, M. (2015). Contrasting leaf phenological strategies optimize carbon gain under droughts of different duration. *Advances in Water Resources*, *84*, 37-51.

Maréchaux, Isabelle, Megan K. Bartlett, Lawren Sack, Christopher Baraloto, Julien Engel, Emilie Joetzjer, and Jérôme Chave. 2015. “Drought Tolerance as Predicted by Leaf Water Potential at Turgor Loss Point Varies Strongly Across Species Within an Amazonian Forest.” Edited by Kaoru Kitajima. Functional Ecology 29 (10): 1268–77. https://doi.org/10.1111/1365-2435.12452.

Maréchaux, Isabelle, Laurent Saint-André, Megan K. Bartlett, Lawren Sack, and Jérôme Chave. 2019. “Leaf Drought Tolerance Cannot Be Inferred from Classic Leaf Traits in a Tropical Rainforest.” Edited by Pierre Mariotte. Journal of Ecology 108 (3): 1030–45. https://doi.org/10.1111/1365-2745.13321.

Maréchaux, I., Langerwisch, F., Huth, A., Bugmann, H., Morin, X., Reyer, C. P., ... & Bohn, F. J. (2021). Tackling unresolved questions in forest ecology: The past and future role of simulation models. *Ecology and Evolution*, *11*(9), 3746-3770.

McMahon, S. M., Harrison, S. P., Armbruster, W. S., Bartlein, P. J., Beale, C. M., Edwards, M. E., Kattge, J., Midgley, G., Morin, X., and Prentice, I. C.: Improving assessment and modelling of climate change impacts on global terrestrial biodiversity, Trends in Ecology & Evolution, 26, 249–259, https://doi.org/10.1016/j.tree.2011.02.012, 2011.

Medlyn, B. E., Robinson, A. P., Clement, R., & McMurtrie, R. E. (2005). On the validation of models of forest CO2 exchange using eddy covariance data: some perils and pitfalls. *Tree physiology*, *25*(7), 839-857.

Medlyn, B. E., Duursma, R. A., De Kauwe, M. G., & Prentice, I. C. (2013). The optimal stomatal response to atmospheric CO2 concentration: Alternative solutions, alternative interpretations. Agricultural and Forest Meteorology, 182, 200-203.

Meir, P., Grace, J. & Miranda, A.C. (2000). Photographic method to measure the vertical distribution of leaf area density in forests. *Agricultural and Forest Meteorology*, **102**, 105–111.

Merganičová, K., Merganič, J., Lehtonen, A., Vacchiano, G., Sever, M. Z. O., Augustynczik, A. L., ... & Reyer, C. P. (2019). Forest carbon allocation modelling under climate change. *Tree Physiology*, *39*(12), 1937-1960.

Meunier, F., Verbruggen, W., Verbeeck, H., & Peaucelle, M. (2022). Low sensitivity of three terrestrial biosphere models to soil texture over the South American tropics. *Geoscientific Model Development*, *15*(20), 7573-7591.

Mokany, K., Ferrier, S., Connolly, S. R., Dunstan, P. K., Fulton, E. A., Harfoot, M. B., ... & Wintle, B. A. (2016). Integrating modelling of biodiversity composition and ecosystem function. *Oikos*, *125*(1), 10-19.

Moorcroft, P. R., Hurtt, G. C., and Pacala, S. W.: A method for scaling vegetation dynamics: the ecosystem demography model (ed), Ecological Monographs, 71, 557–586, https://doi.org/10.1890/0012-9615(2001)071[0557:AMFSVD]2.0.CO;2, 2001.

Muller-Landau, H. C. (2010). The tolerance–fecundity trade-off and the maintenance of diversity in seed size. *Proceedings of the National Academy of Sciences*, *107*(9), 4242-4247.

Muñoz-Sabater, Joaquín, Emanuel Dutra, Anna Agustí-Panareda, Clément Albergel, Gabriele Arduini, Gianpaolo Balsamo, Souhail Boussetta, et al. 2021. "ERA5-Land: A State-of-the-Art Global Reanalysis Dataset for Land Applications." Earth System Science Data 13 (9): 4349–83. https://doi.org/10.5194/essd-13-4349-2021.

Nemetschek, Daniela, Géraldine Derroire, Eric Marcon, Mélaine Aubry-Kientz, Johanna Auer, Vincyane Badouard, Christopher Baraloto, et al. 2024. "Climate Anomalies and Neighbourhood Crowding Interact in Shaping Tree Growth in Old-Growth and Selectively Logged Tropical Forests." Journal of Ecology, January. https://doi.org/10.1111/1365-2745.14256.

Nepstad, D. C., P. Moutinho, M. B. Dias-Filho, E. Davidson, G. Cardinot, D. Markewitz, R. Figueiredo, et al. 2002. "The Effects of Partial Throughfall Exclusion on Canopy Processes, Aboveground Production, and Biogeochemistry of an Amazon Forest." Journal of Geophysical Research: Atmospheres 107 (D20). https://doi.org/10.1029/2001jd000360.

Nunes, M. H., Camargo, J. L. C., Vincent, G., Calders, K., Oliveira, R. S., Huete, A., ... & Maeda, E. E. (2022). Forest fragmentation impacts the seasonality of Amazonian evergreen canopies. *Nature Communications*, 13(1), 917.

Paschalis, A., De Kauwe, M. G., Sabot, M., and Fatichi, S.: When do plant hydraulics matter in terrestrial biosphere modelling?, Global Change Biology, 30, e17022, https://doi.org/10.1111/gcb.17022, 2024.

Pastorello, Gilberto, Trotta, Carlo, Canfora, Eleonora, Chu, Housen, Christianson, Danielle, Cheah, You-Wei, Poindexter, Cristina, et al. 2020. "The FLUXNET2015 Dataset and the ONEFlux Processing Pipeline for Eddy Covariance Data." Nature Publishing Group. https://doi.org/10.5167/UZH-190509.

Poorter, L., Oberbauer, S. F., & Clark, D. B. (1995). Leaf optical properties along a vertical gradient in a tropical rain forest canopy in Costa Rica. *American Journal of Botany*, *82*(10), 1257-1263.

Powell, T. L., Galbraith, D. R., Christoffersen, B. O., Harper, A., Imbuzeiro, H. M. A., Rowland, L., Almeida, S., Brando, P. M., da Costa, A. C. L., Costa, M. H., Levine, N. M., Malhi, Y., Saleska, S. R., Sotta, E., Williams, M., Meir, P., and Moorcroft, P. R.: Confronting model predictions of carbon fluxes with measurements of Amazon forests subjected to experimental drought, New Phytologist, 200, 350–365, https://doi.org/10.1111/nph.12390, 2013.

Prentice, I. C., Liang, X., Medlyn, B. E., and Wang, Y.-P.: Reliable, robust and realistic: the three R's of next-generation land-surface modelling, Atmos. Chem. Phys., 15, 5987–6005, https://doi.org/10.5194/acp-15-5987-2015, 2015.

Purves, D. and Pacala, S.: Predictive models of forest dynamics, Science, 320, 1452–1453, https://doi.org/10.1126/science.1155359, 2008.

Quesada, C. A., J. Lloyd, M. Schwarz, S. Patiño, T. R. Baker, C. Czimczik, N. M. Fyllas, et al. 2010. "Variations in Chemical and Physical Properties of Amazon Forest Soils in Relation to Their Genesis." Biogeosciences 7 (5): 1515–41. https://doi.org/10.5194/bg-7-1515-2010.

Qie, L., Lewis, S. L., Sullivan, M. J. P., Lopez-Gonzalez, G., Pickavance, G. C., Sunderland, T., Ashton, P., Hubau, W., Salim, K. A., Aiba, S.-I., Banin, L. F., Berry, N., Brearley, F. Q., Burslem, D. F. R. P., Dančák, M., Davies, S. J., Fredriksson, G., Hamer, K. C., Hédl, R., Kho, L. K., Kitayama, K., Krisnawati, H., Lhota, S., Malhi, Y., Maycock, C., Metali, F., Mirmanto, E., Nagy, L., Nilus, R., Ong, R., Pendry, C. A., Poulsen, A. D., Primack, R. B., Rutishauser, E., Samsoedin, I., Saragih, B., Sist, P., Slik, J. W. F., Sukri, R. S., Svátek, M., Tan, S., Tjoa, A., Nieuwstadt, M. van, Vernimmen, R. R. E., Yassir, I., Kidd, P. S., Fitriadi, M., Ideris, N. K. H., Serudin, R. M., Lim, L. S. A., Saparudin, M. S., and Phillips, O. L.: Long-term carbon sink in Borneo's forests halted by drought and vulnerable to edge effects, Nature Communications, 8, 1966, https://doi.org/10.1038/s41467-017-01997-0, 2017.

Restrepo-Coupe, N., Levine, N. M., Christoffersen, B. O., Albert, L. P., Wu, J., Costa, M. H., Galbraith, D., Imbuzeiro, H., Martins, G., da Araujo, A. C., Malhi, Y. S., Zeng, X., Moorcroft, P., and Saleska, S. R.: Do dynamic global vegetation models capture the seasonality of carbon fluxes in the Amazon basin? A data-model intercomparison, Glob Change Biol, 23, 191–208, https://doi.org/10.1111/gcb.13442, 2017.

Rice, A.H., E. P. Hammond, S. R. Saleska, L. Hutyra, M. Palace, M. Keller, P. B. de Carmargo, K. Portilho, D. Marques and S. C. Wofsy. 2008. LBA-ECO CD-10 Forest Litter Data for km 67 Tower Site, Tapajos National Forest. Data set.

Available on-line [http://daac.ornl.gov] from Oak Ridge National Laboratory Distributed Active Archive Center, Oak Ridge, Tennessee, U.S.A. doi:10.3334/ORNLDAAC/862

Ross, J. (1981). The radiation regime and architecture of plant stands. The Hague: Dr. W. Junk Publishers doi, 10, 978-94.

Rutishauser, E., Wagner, F., Herault, B., Nicolini, E. A., & Blanc, L. (2010). Contrasting above-ground biomass balance in a Neotropical rain forest. *Journal of Vegetation Science*, *21*(4), 672-682.

Sabatier, Daniel, Michel Grimaldi, Marie-Françoise Prévost, Julie Guillaume, Michel Godron, Mireille Dosso, and Daniel Sabatier. 1997. "The Influence of Soil Cover Organization on the Floristic and Structural Heterogeneity of a Guianan Rain Forest." Plant Ecology Formerly "Vegetatio" 131 (1): 81–108. https://doi.org/10.1023/a:1009775025850.

Sabot, M. E., De Kauwe, M. G., Pitman, A. J., Medlyn, B. E., Ellsworth, D. S., Martin-StPaul, N. K., ... & Serbin, S. P. (2022). One stomatal model to rule them all? Toward improved representation of carbon and water exchange in global models. *Journal of Advances in Modeling Earth Systems*, *14*(4), e2021MS002761.

Sakschewski, B., von Bloh, W., Boit, A., Rammig, A., Kattge, J., Poorter, L., Peñuelas, J., and Thonicke, K.: Leaf and stem economics spectra drive diversity of functional plant traits in a dynamic global vegetation model, Glob Change Biol, 21, 2711–2725, https://doi.org/10.1111/gcb.12870, 2015.

Saleska, S. R., Miller, S. D., Matross, D. M., Goulden, M. L., Wofsy, S. C., Da Rocha, H. R., ... & Silva, H. (2003). Carbon in Amazon forests: unexpected seasonal fluxes and disturbance-induced losses. *Science*, *302*(5650), 1554-1557.

Scheiter, S., Langan, L., and Higgins, S. I.: Next-generation dynamic global vegetation models: learning from community ecology, New Phytol, 198, 957–969, https://doi.org/10.1111/nph.12210, 2013.

Schmitt, Sylvain, and Marion Boisseaux. 2023. "Higher Local Intra- Than Interspecific Variability in Water- and Carbon-Related Leaf Traits Among Neotropical Tree Species." Annals of Botany 131 (5): 801–11. https://doi.org/10.1093/aob/mcad042.

Schmitt, Sylvain, Guillaume Salzet, Fabian Jörg Fischer, Isabelle Maréchaux, and Jerome Chave. 2023. "Rcontroll: An R Interface for the Individual-Based Forest Dynamics Simulator TROLL." Methods in Ecology and Evolution 14 (11): 2749–57. https://doi.org/10.1111/2041-210x.14215.

Silver, Whendee L., Jason Neff, Megan McGroddy, Ed Veldkamp, Michael Keller, and Raimundo Cosme. 2000. "Effects of Soil Texture on Belowground Carbon and Nutrient Storage in a Lowland Amazonian Forest Ecosystem." Ecosystems 3 (2): 193–209. https://doi.org/10.1007/s100210000019.

Smith, B., Prentice, I. C., and Sykes, M. T.: Representation of vegetation dynamics in the modelling of terrestrial ecosystems: comparing two contrasting approaches within European climate space, Global Ecology and Biogeography, 10, 621–637, https://doi.org/10.1046/j.1466-822X.2001.t01-1-00256.x, 2001.

Smith, Marielle N., Scott C. Stark, Tyeen C. Taylor, Mauricio L. Ferreira, Eronaldo de Oliveira, Natalia Restrepo-Coupe, Shuli Chen, et al. 2019. "Seasonal and Drought-Related Changes in Leaf Area Profiles Depend on Height and Light Environment in an Amazon Forest." New Phytologist 222 (3): 1284–97. https://doi.org/10.1111/nph.15726.

Thuiller, W., Albert, C., Araújo, M. B., Berry, P. M., Cabeza, M., Guisan, A., Hickler, T., Midgley, G. F., Paterson, J., Schurr, F. M., Sykes, M. T., and Zimmermann, N. E.: Predicting global change impacts on plant species' distributions: Future challenges, Perspectives in Plant Ecology, Evolution and Systematics, 9, 137–152, https://doi.org/10.1016/j.ppees.2007.09.004, 2008.

Trugman, A. T., Medvigy, D., Mankin, J. S., and Anderegg, W. R. L.: Soil Moisture Stress as a Major Driver of Carbon Cycle Uncertainty, Geophysical Research Letters, 45, 6495–6503, https://doi.org/10.1029/2018GL078131, 2018.

Van Langenhove, Leandro, Thomas Depaepe, Lore T. Verryckt, Helena Vallicrosa, Lucia Fuchslueger, Laynara F. Lugli, Laëtitia Bréchet, et al. 2021. "Impact of Nutrient Additions on Free-Living Nitrogen Fixation in Litter and Soil of Two French-Guianese Lowland Tropical Forests." Journal of Geophysical Research: Biogeosciences 126 (7). https://doi.org/10.1029/2020jg006023.

Ukkola, A. M., Abramowitz, G., & De Kauwe, M. G. PLUMBER2: forcing and evaluation datasets for a model intercomparison project for land surface models v1. 0, Geonetwork [data set].

Van Bodegom, P. M., Douma, J. C., and Verheijen, L. M.: A fully traits-based approach to modeling global vegetation distribution, PNAS, 111, 13733–13738, https://doi.org/10.1073/pnas.1304551110, 2014.

Van Buuren, S., & Groothuis-Oudshoorn, K. (2011). mice: Multivariate imputation by chained equations in R. *Journal of statistical software*, *45*, 1-67.

Van Langenhove, L., Verryckt, L. T., Bréchet, L., Courtois, E. A., Stahl, C., Hofhansl, F., ... & Janssens, I. A. (2020). Atmospheric deposition of elements and its relevance for nutrient budgets of tropical forests. *Biogeochemistry*, *149*, 175-193.

Villarreal, S., & Vargas, R. (2021). Representativeness of FLUXNET sites across Latin America. *Journal of Geophysical Research: Biogeosciences*, *126*(3), e2020JG006090.

Vincent, G., Antin, C., Laurans, M., Heurtebize, J., Durrieu, S., Lavalley, C., & Dauzat, J. (2017). Mapping plant area index of tropical evergreen forest by airborne laser scanning. A cross-validation study using LAI2200 optical sensor. *Remote Sensing of Environment*, *198*, 254-266.

Vincent, G., Pimont, F., Verley, P., 2021. A note on PAD/LAD estimators implemented in AMAPVox 1.8. https://doi.org/10.23708/1AJNMP

Vincent, G., Verley, P., Brede, B., Delaitre, G., Maurent, E., Ball, J., ... & Barbier, N. (2023). Multi-sensor airborne lidar requires intercalibration for consistent estimation of light attenuation and plant area density. *Remote Sensing of Environment*, *286*, 113442.

Vleminckx, Jason, Claire Fortunel, Oscar Valverde-Barrantes, C. E. Timothy Paine, Julien Engel, Pascal Petronelli, Aurélie K. Dourdain, Juan Guevara, Solène Béroujon, and Christopher Baraloto. 2021. "Resolving Whole-Plant Economics from Leaf, Stem and Root Traits of 1467 Amazonian Tree Species." Oikos 130 (7): 1193–1208. https://doi.org/10.1111/oik.08284.

Wagner, F. H., Hérault, B., Bonal, D., Stahl, C., Anderson, L. O., Baker, T. R., ... & Aragão, L. E. (2016). Climate seasonality limits leaf carbon assimilation and wood productivity in tropical forests. *Biogeosciences*, 13(8), 2537-2562.

Wu, J., Albert, L. P., Lopes, A. P., Restrepo-Coupe, N., Hayek, M., Wiedemann, K. T., ... & Saleska, S. R. (2016). Leaf development and demography explain photosynthetic seasonality in Amazon evergreen forests. *Science*, *351*(6276), 972-976.

Wu, J., Serbin, S. P., Xu, X., Albert, L. P., Chen, M., Meng, R., ... & Rogers, A. (2017). The phenology of leaf quality and its within-canopy variation is essential for accurate modeling of photosynthesis in tropical evergreen forests. *Global Change Biology*, *23*(11), 4814-4827.

Wu, W., Sun, Y., Xiao, K., & Xin, Q. (2021). Development of a global annual land surface phenology dataset for 1982–2018 from the AVHRR data by implementing multiple phenology retrieving methods. *International Journal of Applied Earth Observation and Geoinformation*, *103*, 102487.

Yang, X., Wu, J., Chen, X., Ciais, P., Maignan, F., Yuan, W., ... & Wright, S. J. (2021). A comprehensive framework for seasonal controls of leaf abscission and productivity in evergreen broadleaved tropical and subtropical forests. *The Innovation*, *2*(4).

Yang, Xueqin, Xiuzhi Chen, Jiashun Ren, Wenping Yuan, Liyang Liu, Juxiu Liu, Dexiang Chen, et al. 2023. "A Grid Dataset of Leaf Age-Dependent LAI Seasonality Product (Lad-LAI) over Tropical and Subtropical Evergreen Broadleaved Forests." http://dx.doi.org/10.5194/essd-2022-436.

Yao, Y., Ciais, P., Viovy, N., Joetzjer, E., and Chave, J.: How drought events during the last century have impacted biomass carbon in Amazonian rainforests, Global Change Biology, 29, 747–762, https://doi.org/10.1111/gcb.16504, 2023.

Ziegler, C., Coste, S., Stahl, C., Delzon, S., Levionnois, S., Cazal, J., ... & Bonal, D. (2019). Large hydraulic safety margins protect Neotropical canopy rainforest tree species against hydraulic failure during drought. Annals of Forest Science, 76, 1-18.

TROLL 4.0: an individual- and trait-based forest dynamics model to jointly simulate tropical forest structure, diversity, and ecosystem functioning – Part 2: Model evaluation for two Amazonian sites

Sylvain Schmitt et al.

Correspondence to: Sylvain Schmitt (sylvain.schmitt@cirad.fr)

Table S1: TROLL 4.0 global parameters.

Abbreviation	Definition	Units	Value	Nature*	Reference
c_a	Carbon free air concentration	$\mu mol\ mol^{-1}$	375	Constant	
P_{ress}	Atmospheric pressure	kPa	101	Constant	
k_{geom}	Light extinction coefficient, reflecting leaf geometric arrangement	unitless	0.5	Constant	Ross 1981
$absorptance_{leaves}$	leaves absorptance	unitless	0.83	Literature	Long et al., 1993; Poorter et al., 1995
θ	Curvature factor (Farquhar model parameter)	unitless	0.7	Literature	Farquhar et al., 1980
g_0	leaf minimum conductance for water vapor	mmol H_20 m^{-2} s^{-1}	5	Literature	Duursma et al., 2019
$a_{T,o}$	Phenological parameter that modulates old leaf drought tolerance	unitless		Calibrated	
$b_{T,o}$	Phenological parameter that modulates the height dependence of leaf susceptibility to drought	MPa		Calibrated	

δ_o	Phenological parameter that controls the pace of old leaf shedding acceleration	unitless			Calibrated	
f_{wood}	Fraction of carbon allocated to wood	unitless		0.35	Literature	Aragão et al., 2019; Malhi et al., 2011
f_{canopy}	Fraction of carbon allocated to canopy			0.25	Literature	Aragão et al., 2019; Malhi et al., 2011
f_{gap}	Fraction of gaps in the tree crown			0.15	Literature	Fischer et al., 2019
a_{CR}	Crown radius intercept	unitless			Calibrated	
b_{CR}	Crown radius slope	unitless			Calibrated	
a_{CD}	Crown depth intercept		m	0	Literature	Chave et al., 2005
b_{CD}	Crown depth slope	unitless		0.2	Literature	Chave et al., 2005
$shape_{crown}$	Crown shape parameter			0.72	Calibrated	
N_{tot}	Intensity of the external seed rain		$seeds\ ha^{-1}$	50,000	Assumed	
n_s	Number of reproduction opportunities per mature tree		$seeds\ tree^{-1}$	10	Assumed	
m	Reference background mortality		$death\ year^{-1}$		Calibrated	
v_T	Variance of the flexion moment for treefall			0.021	Calibrated	
σ_h	Intraspecific variation in height (log scale)		m	0.19	Inferred	Baraloto et al., 2010
σ_{cr}	Intraspecific variation in crown radius (log scale)		m	0.29	Calibrated	Fischer et al., 2019
σ_{cd}	Intraspecific variation in crown depth (log scale)		m	0		

σ_{dbhmax}	Intraspecific variation in maximum diameters (log scale)	m	0.05	Inferred	Baraloto et al., 2010
$corr_{cr-h}$	Intraspecific correlation between crown radius and height		0		
σ_P	Intraspecific variation in phosphorus (log scale)	$mg.g^{-1}$	0.24	Inferred	Baraloto et al., 2010
σ_N	Intraspecific variation in nitrogen (log scale)	$mg.g^{-1}$	0.12	Inferred	Baraloto et al., 2010
σ_{LMA}	Intraspecific variation in leaf mass per area (log scale)	$g.m^{-2}$	0.24	Inferred	Baraloto et al., 2010
σ_{wsg}	Intraspecific variation in wood specific gravity	$g.cm^{-3}$	0.06	Inferred	Baraloto et al., 2010
σ_{LA}	Intraspecific variation in leaf area (log scale)	cm^2	0.48	Inferred	Schmitt and Boisseaux 2023
σ_{tlp}	Intraspecific variation in turgor loss point (log scale)	MPa	0.10	Inferred	Schmitt and Boisseaux 2023
$corr_{N-P}$	Intraspecific correlation between nitrogen and phosphorous		0.65	Inferred	Baraloto et al., 2010
$corr_{N-LMA}$	Intraspecific correlation between nitrogen and leaf mass per area		-0.43	Inferred	Baraloto et al., 2010
$corr_{P-LMA}$	Intraspecific correlation between phosphorus and leaf mass per area		-0.39	Inferred	Baraloto et al., 2010

*Assumed is a value that is supposed; Calibrated is a value that was previously calibrated; Constant is a fundamental physic constant; Literature is a value prescribed from the literature.

Table S2: Evaluation of forest structure, composition and fluxes explored at Paracou and Tapajos. Evaluations include the goodness-of-fit R^2 from the linear regression with a null intercept, the Pearson's r correlation coefficient CC, the root mean square error of prediction RMSEP, the standard deviation of the error of prediction SD.

Site	Variable	Unit	Observations	Temporal resolution	R^2	CC	RMSEP	SD
Paracou	height	%	Plane	single	0.93	0.95	0.76	0.76
Tapajos	height	%	Plane	single	0.94	0.94	0.56	0.55
Paracou	height	%	Satellite	single	0.95	0.96	0.55	0.55
Tapajos	height	%	Satellite	single	0.92	0.91	0.69	0.62
Paracou	BA understory	$m^2.ha^{-1}$	Inventory	single	0.94	0.90	0.12	0.08
Paracou	Abundance understory	ha^{-1}	Inventory	single	0.99	1.00	342.15	309.81
Paracou	Rank-abundance	ha^{-1}	Inventory	single	0.85	0.93	3.67	3.58
Tapajos	Rank-abundance	ha^{-1}	Inventory	single	0.74	0.94	3.63	3.48
Paracou	GPP	$kgC.m^{-2}.yr^{-1}$	Eddy-flux	day	0.97	0.60	0.75	0.67
Tapajos	GPP	$kgC.m^{-2}.yr^{-1}$	Eddy-flux	day	0.97	0.45	1.12	0.67
Paracou	GPP	$kgC.m^{-2}.yr^{-1}$	Satellite	day	0.95	0.45	1.18	0.80
Tapajos	GPP	$kgC.m^{-2}.yr^{-1}$	Satellite	day	0.96	0.22	1.54	0.28
Paracou	LAI	$m^2.m^{-2}$	Satellite	15 days	1.00	0.69	0.29	0.13
Tapajos	LAI	$m^2.m^{-2}$	Satellite	15 days	1.00	0.55	0.26	0.17
Paracou	LAI	$m^2.m^{-2}$	Drone	15 days	1.00	0.84	0.11	0.11
Tapajos	LAI	$m^2.m^{-2}$	Terrestrial	15 days	1.00	0.25	0.32	0.20
Tapajos	LAI	$m^2.m^{-2}$	Phenocam	15 days	1.00	0.91	0.11	0.08
Paracou	ET	$mm.day^{-1}$	Eddy-flux	day	0.96	0.69	0.60	0.60
Tapajos	ET	$mm.day^{-1}$	Eddy-flux	day	0.96	0.75	0.75	0.63
Paracou	RSWC	%	Eddy-flux	day	0.97	0.77	0.24	0.13

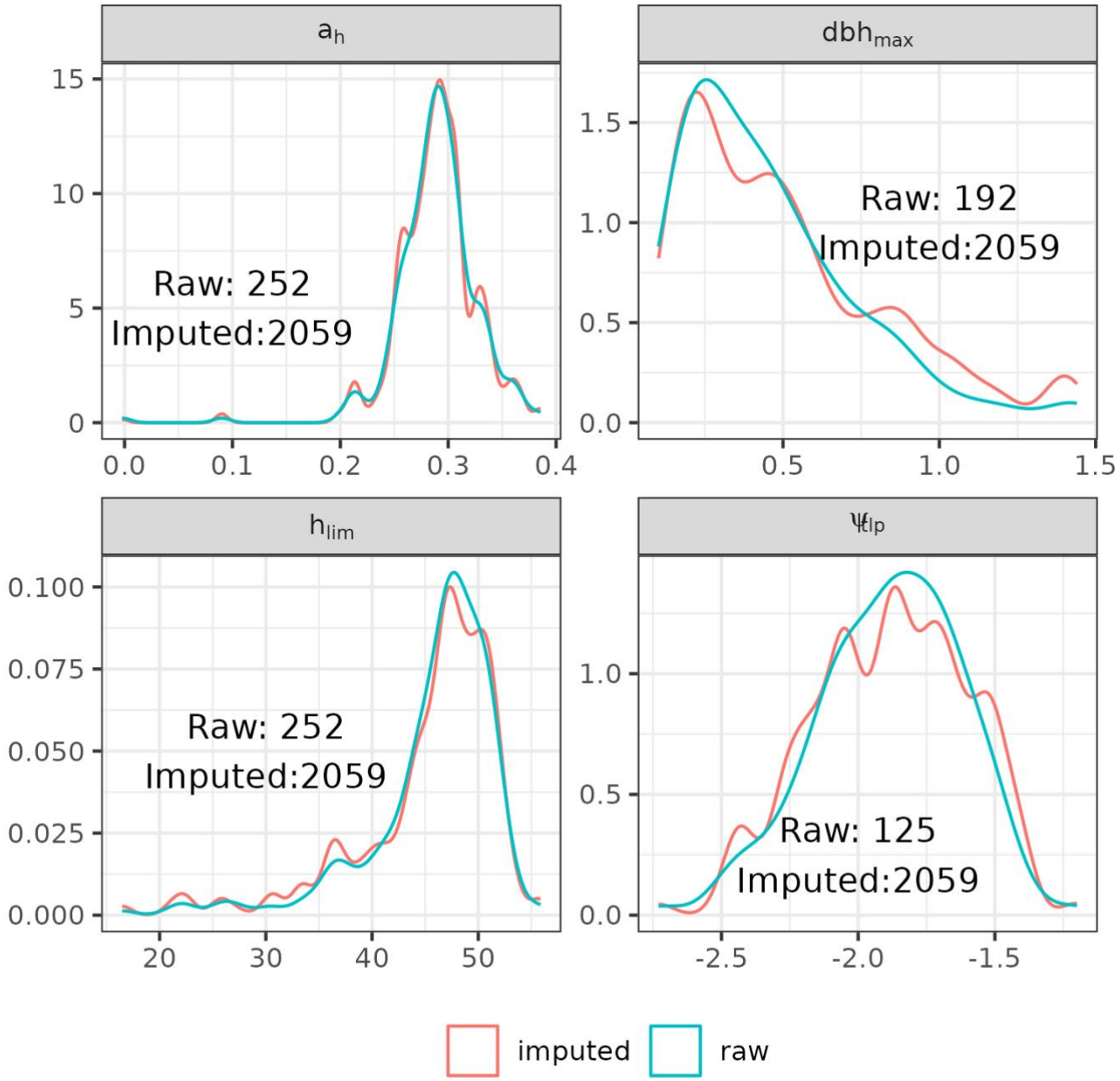

Figure S1: Representativity of imputed functional traits values (red) against raw functional trait values (blue) from various datasets (see methods). Traits were imputed using predictive means matching for dbh_{max}, hlim, and ψ_{tlp} only. The number in each subplots represents the number of species with a trait value in the raw data and after imputation composing respectively the blue and red curves.

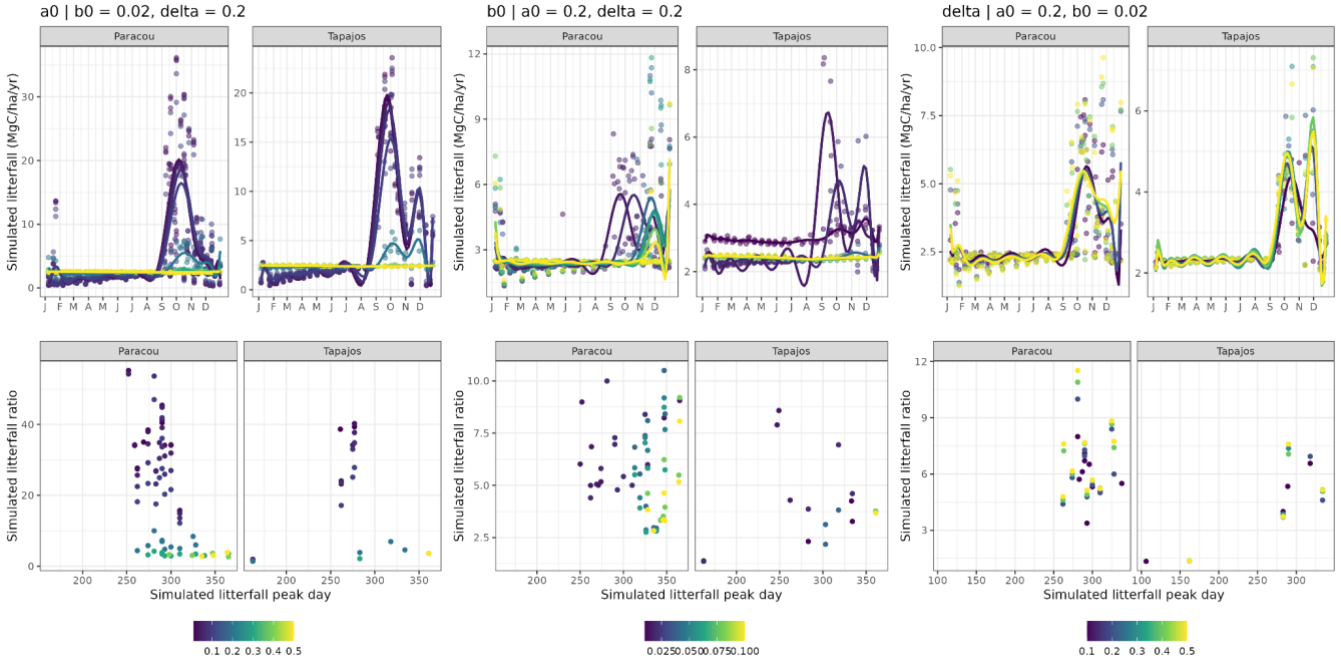

Figure S2. Effect of each parameter of the new leaf shedding module on the simulated timing and intensity of the litterfall peak during the dry season. Top panels illustrate simulated variations of litterfall at both sites for varying $a_{T,0}$, $b_{T,0}$, and δ_0 with the other parameters fixed to a calibrated value. Bottom panels illustrate the corresponding timing and intensity of the dry season litterfall peak: (i) the day of the litterfall peak as the julian day of the maximum annual value (day), and (ii) the ratio between the peak value (computed as the average of litterfall flux over the two consecutive time intervals before and after the peak day) divided by the basal flux (computed as the average between January and April) (ratio). $a_{T,0}$ mainly limited the intensity of the peak with a peak up to 60 times the wet season base litter flux with small parameter values close to 0.01 and no peak with values greater than 0.3, when $b_{T,0}$=0.02 and δ_0 =0.2. Values of $a_{T,0}$ greater than 0.1 also resulted in a later peak during the dry season. $b_{T,0}$ mainly influenced the date of the simulated peak during the dry season, as well as the intensity of the simulated peak for values greater than 0.1. Indeed, low values of $b_{T,0}$, close to 0.01, resulted in a peak starting in September, while high values showed a peak starting in December, when $a_{T,0}$=0.2 and δ_0=0.2. Finally, δ_0 appeared to have a smaller influence on the intensity and timing of the simulated litter peaks. Higher values of δ_0 increased the duration of the simulated peaks or the litter flux between two peaks during the same dry season.

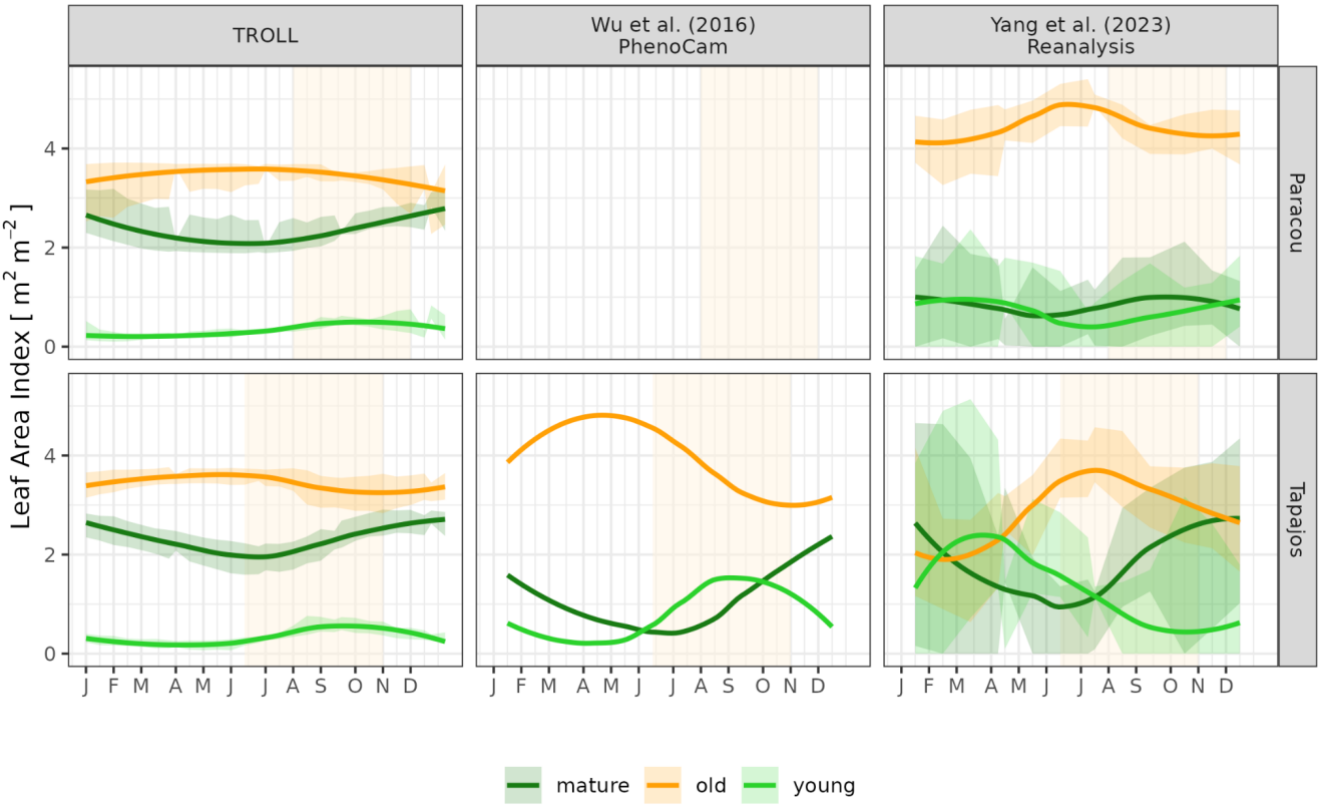

Figure S3: Mean annual cycle of leaf area index per leaf age cohorts, derived from fortnightly means, at Paracou and Tapajos. Note that the three leaf age cohorts (young, mature and old leaves) are not defined the same way in the three sources. Leaf age per cohort depends on the individual leaf lifespan in TROLL 4.0 (see Maréchaux et al., submitted companion paper), while the transition from young to mature and mature to old are respectively fixed to 1.71 and 5.14 months in Yang et al. (2023) and fitted to 1 and 3 months in Wu et al. (2016). Bands are the intervals of means across years, and the vertical yellow bands in the background correspond to the site's climatological dry season.

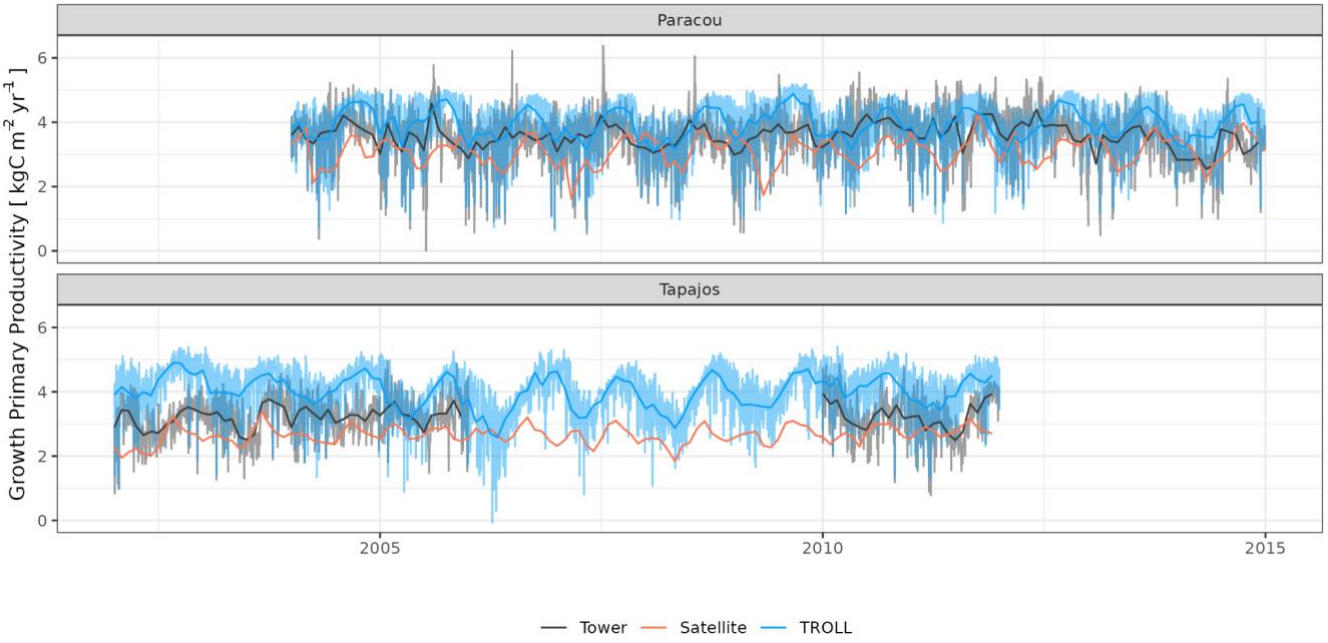

Figure S4: Daily and monthly means of gross primary productivity for Paracou and Tapajos. Dark lines are the monthly means, semi-transparent lines are the daily means variations with the exception of satellite data for which data are available only every 8 days.

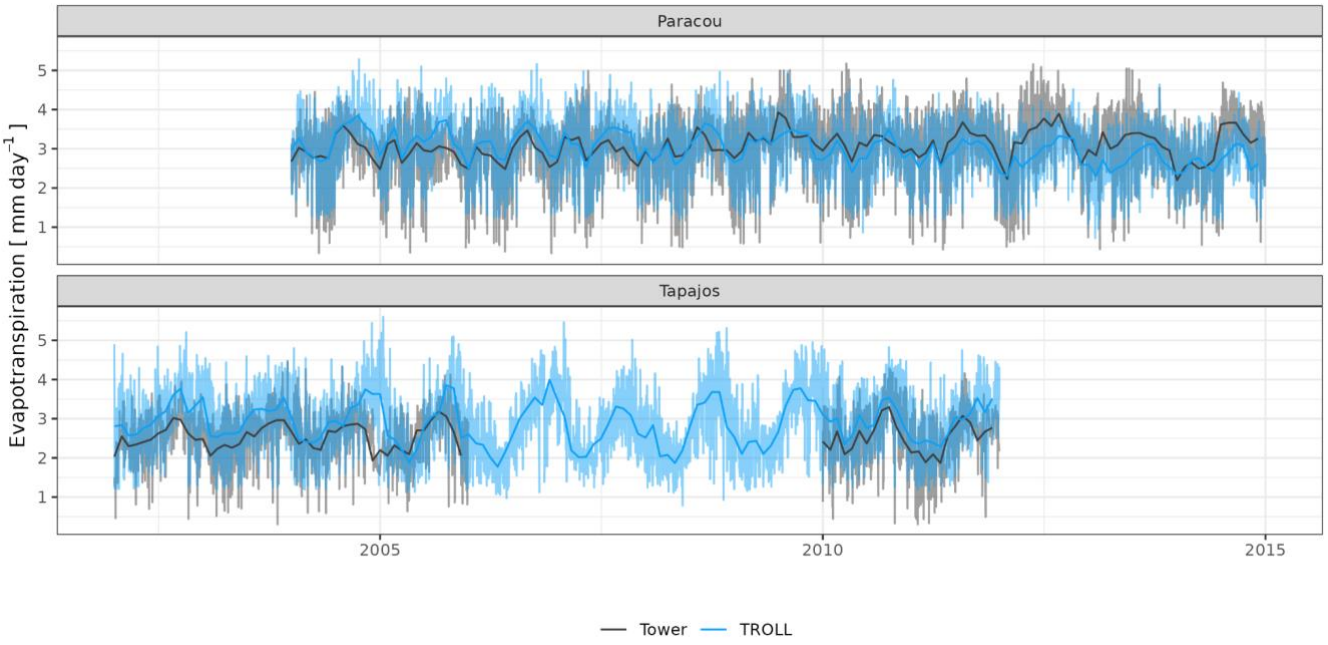

Figure S5: Daily and monthly total of evapotranspiration for Paracou and Tapajos. Dark lines are the monthly means, semi-transparent lines are the daily means variations.

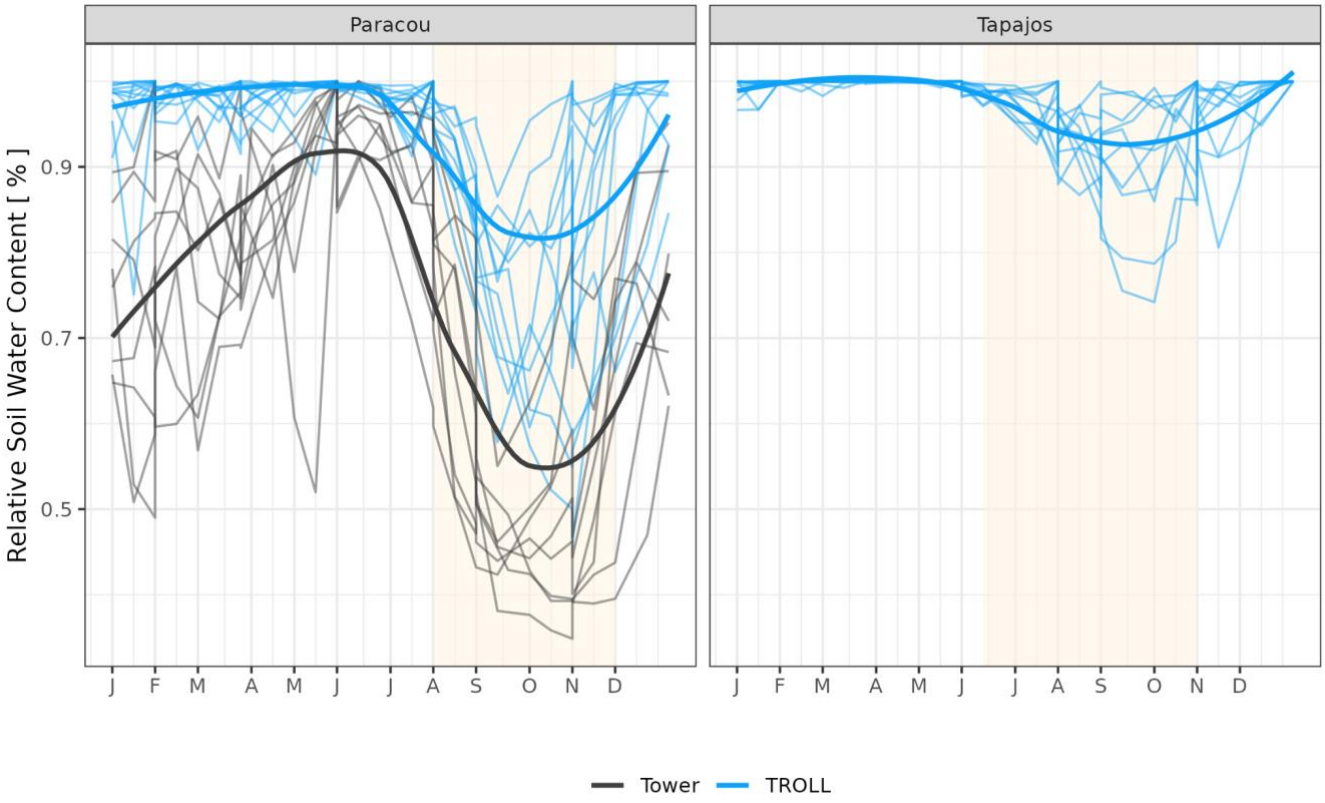

Figure S6: Mean annual cycle from daily means of relative soil water content for Paracou and Tapajos for the topsoil layer up to 10 cm. Dark lines are the daily mean across years, semi-transparent lines are the daily means per year. The vertical yellow bands in the background correspond to the site's climatological dry season.

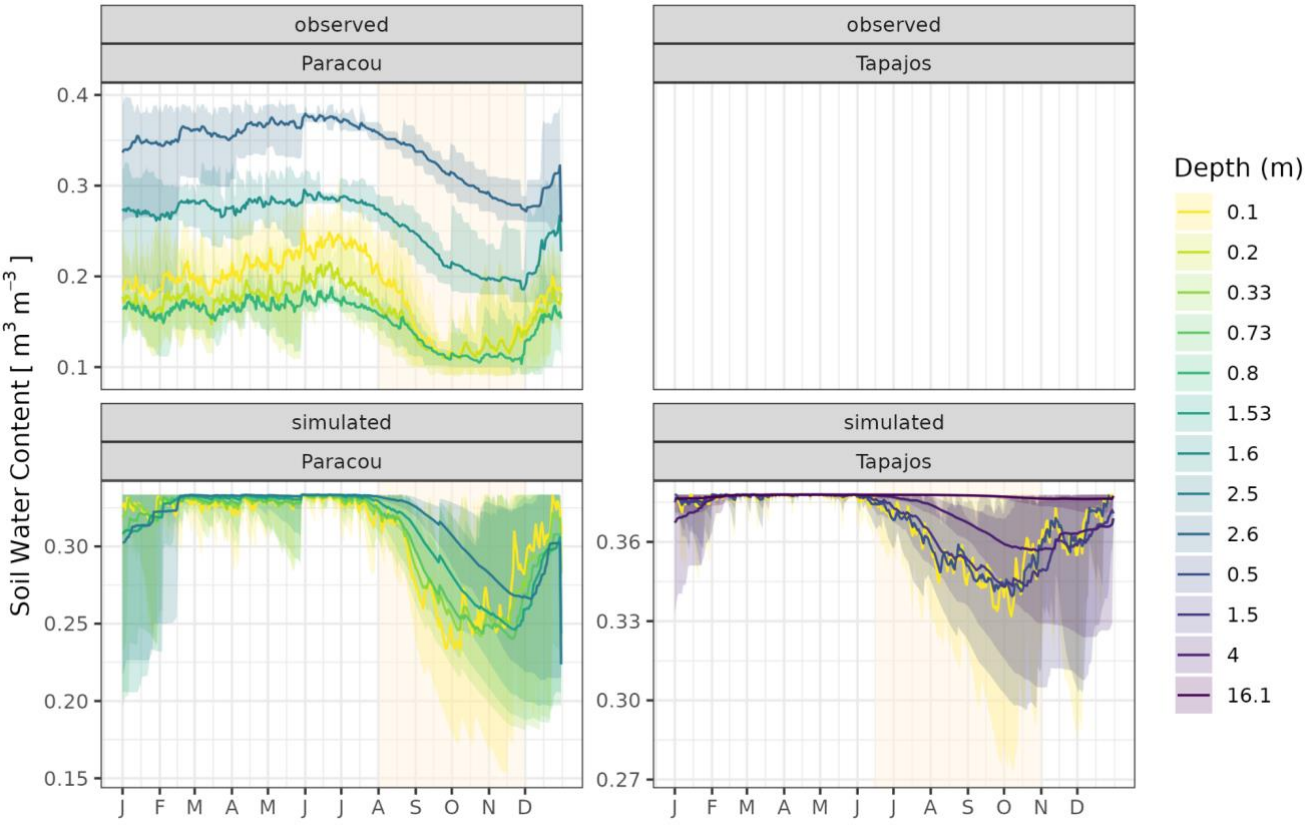

Figure S7: Mean annual cycle from daily means of soil water content for Paracou and Tapajos at different depths. The depth value indicates the maximum depth of the layer. Dark lines are the daily means across years, and bands are the intervals of means across ten years The vertical yellow bands in the background correspond to the site's climatological dry season.